

# Geometrical Constraints on Finite-time Lyapunov Exponents in Two and Three Dimensions

Jean-Luc Thiffeault and Allen H. Boozer

*Columbia University, Department of Applied Physics and Applied Mathematics,  
New York, NY 10027*

## Abstract

Constraints are found on the spatial variation of finite-time Lyapunov exponents of two- and three-dimensional systems of ordinary differential equations. In a chaotic system, finite-time Lyapunov exponents describe the average rate of separation, along characteristic directions, of neighboring trajectories. The solution of the equations is a coordinate transformation that takes initial conditions (the Lagrangian coordinates) to the state of the system at a later time (the Eulerian coordinates). This coordinate transformation naturally defines a metric tensor, from which the Lyapunov exponents and characteristic directions are obtained. By requiring that the Riemann curvature tensor vanish for the metric tensor (a basic result of differential geometry in a flat space), differential constraints relating the finite-time Lyapunov exponents to the characteristic directions are derived. These constraints are realized with exponential accuracy in time. A consequence of the relations is that the finite-time Lyapunov exponents are locally small in regions where the curvature of the stable manifold is large, which has implications for the efficiency of chaotic mixing in the advection–diffusion equation. The constraints also modify previous estimates of the asymptotic growth rates of quantities in the dynamo problem, such as the magnitude of the induced current.

*Published in Chaos* **11**, 16-28 (2001). *Copyright 2001 American Institute of Physics*

**In a dynamical system, the average rate of stretching of infinitesimal elements of phase-space is described by the Lyapunov exponents. For a fluid, this stretching is crucial to the enhanced diffusion observed in chaotic flows. Though the exponents converge to a time-asymptotic limit that is independent of the initial condition, in most situations of interest this convergence is very slow: there exist regions where, for finite times, the exponents remain anomalously small. Information on the spatial and temporal behavior of finite-time Lyapunov exponents is thus useful in identifying such regions of low stretching rates. Our approach is to regard the time evolution of the solution to a set of ordinary differential equations as a coordinate transformation. For smooth dynamical systems, we**

can study this transformation with the tools of differential geometry. Specifically, we consider the Riemann curvature tensor, a quantity that must vanish in every coordinate system when using the usual Euclidean distance. By examining the details of how the different terms of the Riemann tensor balance each other, we obtain constraints on the finite-time Lyapunov exponents, clarifying and generalizing previous work.<sup>1,2</sup> These constraints take the form of differential relations between the exponents and the characteristic directions of stretching in the flow. The constraints have implications for chaotic mixing, where they allow identification of locally small finite-time Lyapunov exponents, and for the kinematic dynamo problem, where they imply a slower growth rate of the power needed to sustain a dynamo.

## I. INTRODUCTION

Lyapunov exponents are fundamental to our understanding of chaotic processes. They describe the time-asymptotic rate of separation of neighboring trajectories in a dynamical system, and are global properties of a chaotic region, independent of the trajectory chosen to measure them (the fiducial trajectory). This independence is a consequence of a theorem of Oseledec,<sup>3</sup> which applies in the limit of infinite time. In contrast, the *finite-time* Lyapunov exponents, which describe the instantaneous rate of separation of neighboring trajectories, depend on the choice of fiducial trajectory and so characterize local properties of the chaotic region. Similarly, the characteristic direction of expansion or contraction associated with each exponent is a local property of the chaotic region; it converges exponentially to its time-asymptotic orientation<sup>4,5</sup>—a much more rapid convergence rate than that of the Lyapunov exponents.

The slow convergence of the Lyapunov exponents means that in practical situations, *i.e.*, a computer or laboratory experiment, the system under study only rarely evolves long enough to “feel” the value of the true, infinite-time Lyapunov exponents. Rather, the rates of stretching and contracting of infinitesimal elements of phase-space are dominated by local effects, described by the finite-time Lyapunov exponents. In fluid dynamics and plasma physics, these rates are tied to the strong enhancement of transport observed in chaotic mixing.<sup>6</sup> Thus, the spatial and temporal behavior of the finite-time Lyapunov exponents is worthy of study in its own right, in addition to their time-asymptotic value.

In the present paper we expand upon the work of Tang and Boozer<sup>1,2,7</sup> on the geometrical properties of finite-time Lyapunov exponents. We consider an arbitrary smooth dynamical system, which we take to be a set of ordinary differential equations (ODEs), but could also be a discrete map. For such a system, the solution of the equations of motion is a smooth coordinate transformation (diffeomorphism) from the space of initial conditions (the Lagrangian coordinates, which label a trajectory) to the state of the system at a later time (the Eulerian coordinates). The coordinate transformation is smooth even when the system is chaotic, though it then becomes extremely complicated.

To define Lyapunov exponents, it is necessary to define a norm on the space of our dynamical system, that is, a prescription for measuring distances. This norm is used to quantify the exponential separation of trajectories. The usual choice is the Euclidean norm, a mathematical embodiment of what we intuitively think of as distance. The Euclidean

norm is also the simplest realization of a flat space. In essence, flatness is an intrinsic property of a space that reflects the commutativity of partial derivatives, a fact that is not so trivial in general coordinate systems. Flatness is taken for granted in most numerical and laboratory experiments, as reflected by the use of the Euclidean norm. When a space is not flat, it is said to have curvature; an example is a two-dimensional sphere embedded in three-dimensional space, used in some geophysical models where the atmosphere or the ocean is regarded as very thin. But presently we deal only with flat systems.

A remarkable result of differential geometry is the existence and uniqueness of the Riemann curvature tensor, which vanishes if and only if the underlying space is flat (See Sec. III). The Riemann tensor plays a central role in general relativity, where the curvature of space determines the gravitational forces on matter and light rays. Here, we shall only use curvature as a geometrical property; we make no use of general relativity.

When the Riemann tensor vanishes in one coordinate system (usually, in Cartesian coordinates with the Euclidean norm), it also vanishes in any other coordinate system reached by a smooth transformation.<sup>8</sup> In particular, in a smooth dynamical system the transformation from Lagrangian to Eulerian coordinates leaves a vanishing Riemann tensor invariant. When the system is chaotic, so that trajectories exhibit exponential separation, some terms in the Riemann tensor exhibit exponential growth, while others decrease exponentially. Because the Riemann tensor vanishes identically, these terms have to balance each other; this requires the finite-time Lyapunov exponents and their associated characteristic directions to satisfy certain differential relations, or constraints, as was demonstrated for two-dimensional systems by Tang and Boozer.<sup>1</sup> Under more general conditions and using the orthonormal basis form of the metric tensor,<sup>9</sup> we rederive their constraint and analyze its rate of convergence carefully. We also extend the calculation to three dimensions, confirming a constraint conjectured by Tang and Boozer,<sup>2</sup> as well as deriving new ones. We support our theoretical claims with numerical simulations on two- (oscillating convection rolls<sup>10</sup>) and three-dimensional flows (*ABC* flow<sup>11</sup> and the Lorenz model<sup>12</sup>). We also comment on the possible physical applications of the constraints, specifically to the advection-diffusion equation and the dynamo problem.

The outline of the paper is as follows: in Sec. II we review some basic concepts of differential geometry, as applied to dynamical systems. In Sec. III we focus our attention on the Riemann curvature tensor and its properties. Then, in Sec. IV we examine the nature of the vanishing curvature requirement in two dimensions. We obtain a constraint relating the derivatives of the smallest Lyapunov exponent and the stable direction vector. In Sec. V we carry out the same procedure in three dimensions, deriving three new constraints. We find that a combination of two of these constraints yields the same differential relation as in the two-dimensional case; the persistence of this constraint in three dimensions was conjectured by Tang and Boozer,<sup>2</sup> who were guided by numerical investigation of three-dimensional volume-preserving maps. Finally, in Sec. VI we summarize our results, and discuss possible applications of the constraints.

## II. DIFFERENTIAL GEOMETRY AND DYNAMICAL SYSTEMS

In this section we describe the point of view that the solution of a set of differential equations is a coordinate transformation from the set of initial conditions to the state of

the system at a later time. In that sense, the time evolution is a map of the fluid domain onto itself. Moreover, if we assume that the dynamics are “smooth,” the properties of the coordinate transformation are described by differential geometry. An analysis of these properties is the focus of this paper.

We consider a prescribed smooth two- or three-dimensional vector field given by  $\mathbf{v}(\mathbf{x}, t)$ . For example,  $\mathbf{v}(\mathbf{x}, t)$  could be a fluid flow obtained by a solution of the Navier–Stokes equation, but in general the vector field does not have to correspond to such a fluid flow: it can represent the right-hand side of any smooth system of ordinary differential equations. However, because of the convenient framework provided by a fluid flow, we often refer to the phase space domain of  $\mathbf{x}$  as “the fluid” and to infinitesimal elements of phase space as “fluid elements”.

The *Eulerian* coordinates,  $\mathbf{x}$ , denote the position of a point fixed in the “laboratory” frame. The trajectory of an infinitesimal element of phase space (also called a fluid element by analogy with the fluid-dynamical case) in Eulerian coordinates,  $\mathbf{x}$ , satisfies

$$\frac{\partial \mathbf{x}(\boldsymbol{\xi}, t)}{\partial t} = \mathbf{v}(\mathbf{x}(\boldsymbol{\xi}, t), t), \quad \mathbf{x}(\boldsymbol{\xi}, 0) = \boldsymbol{\xi}, \quad (2.1)$$

where  $\boldsymbol{\xi}$  are the *Lagrangian* coordinates that label fluid elements: they are coordinates that describe a frame moving with the fluid. We have made the usual choice of taking as initial condition  $\mathbf{x}(\boldsymbol{\xi}, 0) = \boldsymbol{\xi}$ , which says that fluid elements are labeled by their initial position; thus, Eulerian and Lagrangian coordinates coincide at  $t = 0$ .

The solution  $\mathbf{x} = \mathbf{x}(\boldsymbol{\xi}, t)$  to Eq. (2.1) is the transformation from Lagrangian ( $\boldsymbol{\xi}$ ) to Eulerian ( $\mathbf{x}$ ) coordinates. For a chaotic flow, this transformation gets extremely complicated as time evolves. However, since we have assumed that  $\mathbf{v}$  is a smooth vector field, the transformation is always differentiable, so that the Jacobian matrix  $\partial x^i / \partial \xi^j$  is well-defined. This allows us to use the tools of differential geometry on the transformation  $\mathbf{x}(\boldsymbol{\xi}, t)$ .

Since our focus is on the rate of separation of neighboring trajectories, as characterized by the Lyapunov exponents, we need to define a way of measuring distances in the Eulerian coordinates, *i.e.*, a *norm* for vectors in the space. The norm we use is the Euclidean norm, defined by  $\|\mathbf{w}\|^2 := \sum_{i=1}^n w^i w^i$ , where  $n$  is the dimension of the space. With this norm, the distance  $ds$  between two infinitesimally separated trajectories  $\mathbf{x}(\boldsymbol{\xi}, t)$  and  $\mathbf{x}(\boldsymbol{\xi} + d\boldsymbol{\xi}, t) = \mathbf{x}(\boldsymbol{\xi}, t) + d\mathbf{x}(\boldsymbol{\xi}, t)$  is

$$ds^2 = \|d\mathbf{x}\|^2 = \sum_{\ell}^n dx^{\ell} dx^{\ell}.$$

We use the chain rule to write this distance in terms of the initial separation  $d\boldsymbol{\xi}$ ,

$$ds^2 = \sum_{\ell, i, j}^n \left( \frac{\partial x^{\ell}}{\partial \xi^i} d\xi^i \right) \left( \frac{\partial x^{\ell}}{\partial \xi^j} d\xi^j \right) = \sum_{i, j}^n g_{ij} d\xi^i d\xi^j,$$

where

$$g_{ij}(\boldsymbol{\xi}, t) := \sum_{\ell=1}^n \frac{\partial x^{\ell}}{\partial \xi^i} \frac{\partial x^{\ell}}{\partial \xi^j}. \quad (2.2)$$

In the terminology of differential geometry, Eq. (2.2) is the flat metric tensor  $\delta_{ij}$  of Eulerian space transformed to Lagrangian coordinates. The metric  $g_{ij}$  is a symmetric, positive-definite matrix that tells us the distance between two infinitesimally separated points in Lagrangian space. Because  $g_{ij}$  is symmetric and positive-definite, it has  $n$  positive real eigenvalues, which we denote by  $\Lambda_\mu(\boldsymbol{\xi}, t)$ , with corresponding orthonormal eigenvectors  $\hat{\mathbf{e}}_\mu(\boldsymbol{\xi}, t)$ ; we can then write the metric in the diagonal form

$$g_{ij}(\boldsymbol{\xi}, t) = \sum_{\mu=1}^n \Lambda_\mu (\hat{e}_\mu)_i (\hat{e}_\mu)_j, \quad (2.3)$$

where  $(\hat{e}_\mu)_i$  is the  $i$ th component of  $\hat{\mathbf{e}}_\mu$ . We assume without loss of generality that  $\Lambda_\mu \geq \Lambda_{\mu+1}$  for  $\mu = 1, \dots, n-1$ . The eigenvectors  $\hat{\mathbf{e}}_\mu$  define directions of initial separations for which neighboring fluid elements are converging or diverging, with  $\Lambda_\mu^{1/2}(\boldsymbol{\xi}, t)$  the distance separating them. It is the rate of exponential growth of these distances that defines the *finite-time Lyapunov exponents* (or characteristic exponents)

$$\lambda_\mu(\boldsymbol{\xi}, t) := \frac{1}{2t} \ln \Lambda_\mu(\boldsymbol{\xi}, t). \quad (2.4)$$

(The factor of  $1/2$  enters because  $ds^2$  is the square of the distance.) In the limit as  $t \rightarrow \infty$ , the finite-time Lyapunov exponents converge to the true Lyapunov exponents,  $\lambda_\mu^\infty$ , which are independent of  $t$  and  $\boldsymbol{\xi}$ .<sup>13</sup> A flow is said to be *chaotic* if at least one of its Lyapunov exponents converges to a positive value. However, this convergence is very slow (logarithmic in time): in practical applications we are almost always dealing with finite-time Lyapunov exponents. For the remainder of this paper, ‘‘Lyapunov exponents’’ refers to the finite-time exponents, unless explicitly denoted as infinite-time. Whereas the Lyapunov exponents converge very slowly, in a chaotic region the characteristic directions  $\hat{\mathbf{e}}_\mu(\boldsymbol{\xi}, t)$  (the eigenvectors of  $g_{ij}$ ) converge rapidly (exponentially fast) to their time-asymptotic value,  $\hat{\mathbf{e}}_\mu^\infty(\boldsymbol{\xi})$ .<sup>4,5</sup>

In the chaotic case, we assume that  $\lambda_1 > 0$  ( $\Lambda_1 > 1$ ) and  $\lambda_n < 0$  ( $\Lambda_n < 1$ ), so that there is at least one exponentially expanding and one exponentially contracting direction. These are referred to as the unstable and stable directions, respectively. In three dimensions, the intermediate exponent  $\lambda_2$  can have either sign. For bounded, autonomous flows (where the velocity field  $\mathbf{v}$  does not depend explicitly on time), the intermediate Lyapunov exponent must converge to zero in the infinite-time limit.<sup>14</sup> For simplicity, we shall often use  $\mu = \{u, m, s\}$  to mean  $\mu = \{1, 2, 3\}$ , and write  $\hat{\mathbf{e}}_\mu = \{\hat{\mathbf{u}}, \hat{\mathbf{m}}, \hat{\mathbf{s}}\}$ . The letters  $\{u, m, s\}$  are abbreviations for ‘‘unstable’’, ‘‘middle’’, and ‘‘stable’’ directions, respectively. In two dimensions, we drop the extraneous middle direction and use  $\mu = \{u, s\}$  to mean  $\mu = \{1, 2\}$ , and write  $\hat{\mathbf{e}}_\mu = \{\hat{\mathbf{u}}, \hat{\mathbf{s}}\}$ .

The existence of a contracting direction in a chaotic flow follows from the assumption that the determinant of  $g_{ij}$

$$g := \det g_{ij} = \prod_{\mu=1}^n \Lambda_\mu \quad (2.5)$$

stays bounded with time; otherwise, the volume of fluid elements grows indefinitely, usually an undesirable situation from the physical standpoint. However, a bounded  $g$  is only a

sufficient condition for the existence of a contracting direction, which often exists without this requirement. Note that  $g = 1$  for incompressible flows ( $\nabla \cdot \mathbf{v} = 0$ ).

In theory, the numerical procedure for finding the characteristic directions and exponents is straightforward: we integrate the ordinary differential equations (2.1) with initial conditions  $\boldsymbol{\xi}$ , together with the set of  $n^2$  equations on the tangent space,

$$\frac{d}{dt} \left( \frac{\partial x^i}{\partial \xi^j} \right) = \sum_{\ell=1}^n \frac{\partial v^i}{\partial x^\ell} \frac{\partial x^\ell}{\partial \xi^j}. \quad (2.6)$$

with initial conditions  $\partial x^i / \partial \xi^j = \delta^i_j$ . The metric is then formed from  $\partial x^i / \partial \xi^j$  using the definition (2.2), and its  $n$  eigenvalues  $\Lambda_\mu$  and eigenvectors  $\hat{\mathbf{e}}_\mu$  are obtained via standard numerical techniques. In practice, for a chaotic flow, the elements of the Jacobian matrix  $\partial x^i / \partial \xi^j$  grow exponentially, and one quickly runs into numerical accuracy problems related to subtracting very large numbers. Many methods have been devised to circumvent this difficulty,<sup>14–17</sup> and we shall use the method of Greene and Kim.<sup>4,5,18</sup> Most methods yield a quantity that differs by a factor proportional to  $1/t$  from the true finite-time Lyapunov exponent, and so need to be corrected.<sup>5,19</sup>

To illustrate the concept of the characteristic directions  $\hat{\mathbf{e}}_\mu$ , let us take the two-dimensional, time-dependent periodic flow,

$$\mathbf{v}_{\text{ocr}} := \left( -\frac{\partial \psi}{\partial x^2}, \frac{\partial \psi}{\partial x^1} \right), \quad \psi(\mathbf{x}, t) := A k^{-1} (\sin kx^1 + \epsilon \cos \omega t \cos kx^1) \sin \pi x^2. \quad (2.7)$$

This flow is incompressible ( $\nabla \cdot \mathbf{v} = 0$ , so that  $g = 1$ ). It is used by many authors (see for example Refs. 10 and 20) to model a periodic set of oscillating convection rolls. The parameters are the amplitude of the rolls,  $A$ , the relative amplitude of the oscillations,  $\epsilon$ , the aspect ratio,  $k$ , and the frequency of oscillations,  $\omega$ . When  $\omega = 0$ , the flow is steady, and the Lagrangian trajectories are nonchaotic. This is true in general of any two-dimensional steady flow.<sup>14</sup>

Figure 1 shows the field of stable directions  $\hat{\mathbf{s}}^\infty$  for the oscillating rolls, Eq. (2.7). The two lines in the figure are portions of stable manifolds, obtained by integrating the set of  $n$  ordinary differential equations

$$\frac{d\boldsymbol{\xi}}{d\tau} = \hat{\mathbf{s}}^\infty(\boldsymbol{\xi}),$$

where  $\tau$  is the arc length along the manifold. In a chaotic flow, the stable manifold comes close to every point in an ergodic region.<sup>14</sup> In Fig. 2 we show a portion of stable manifold for the well-known *ABC* flow [Eq. (5.13)], which we discuss further in Sec. V. The interpretation of the stable manifold is as follows: if two infinitesimally close initial conditions lie on that manifold, their trajectories converge exponentially at a rate  $\lambda_s$ .

Analogous to the stable manifold, there is an unstable manifold corresponding to  $\hat{\mathbf{u}}^\infty$  (and, in three dimensions, a manifold corresponding to  $\hat{\mathbf{m}}^\infty = \hat{\mathbf{s}}^\infty \times \hat{\mathbf{u}}^\infty$ ). The unstable manifold and its relation to mixing have been extensively described in Refs. 21 and 22; an important result is that material lines (*i.e.*, a streak of dye) in a closed flow tends to trace out the unstable manifold.

### III. THE RIEMANN CURVATURE TENSOR

We now apply some well-known results of differential geometry to the metric obtained in Sec. II. The aim is to write the Riemann curvature tensor, which characterizes the flatness of the space, in the basis where the metric tensor in Lagrangian coordinates is diagonal, as defined by Eq. (2.3). In Secs. IV and V, we will use the invariance property of the Riemann tensor and the chaotic nature of the flow to establish constraints on Lyapunov exponents and characteristic directions. We only present the properties of the Riemann tensor that are essential to the argument. For more complete discussions and proofs, we refer the reader to standard textbooks, such as Refs. 9, 23, 24.

Differential geometry tells us that if a metric describes a flat space, then its Riemann curvature tensor

$$R^m{}_{ijk} := \Gamma^m_{ji,k} - \Gamma^m_{ki,j} + \sum_{\ell=1}^n \Gamma^m_{k\ell} \Gamma^\ell_{ji} - \sum_{\ell=1}^n \Gamma^m_{j\ell} \Gamma^\ell_{ki}, \quad (3.1)$$

must vanish in every coordinate system. (A subscript  $k$  following a comma denotes a derivative with respect to the  $k$ th coordinate.) The Christoffel symbols  $\Gamma$  involve derivatives of the metric,

$$\Gamma^i_{jk} := \frac{1}{2} \sum_{\ell=1}^n g^{i\ell} (g_{\ell j,k} + g_{\ell k,j} - g_{jk,\ell}), \quad (3.2)$$

where  $g^{i\ell}$  is the matrix inverse of  $g_{i\ell}$ . The vanishing of the Riemann tensor is equivalent to requiring that second covariant derivatives commute in every coordinate system, a result that is taken for granted in flat space because there covariant derivatives are the same as ordinary derivatives. Covariant derivatives can be thought of as derivatives that take into account a possible spatial dependence of the local coordinate frame.

The Riemann tensor satisfies a number of symmetry properties, so that its total number of independent components is  $n^2(n^2-1)/12$ . In three dimensions, it has six independent components, equivalent to the independent components of the Ricci tensor  $R_{ik} := \sum_{j=1}^n R^j{}_{ijk}$ , which is symmetric. In two dimensions, the Riemann tensor has one independent component, equivalent the Ricci scalar  $R := \sum_{i,k=1}^n g^{ik} R_{ik}$ . In this paper we restrict ourselves to the two- and three-dimensional cases, so we only make use of the Ricci scalar and tensor.

We are interested in finding the components of the Ricci tensor in a frame aligned with the local characteristic directions (the eigenvectors of  $g_{ij}$ , which are orthonormal). The calculation of the Riemann tensor in such an orthonormal basis<sup>25</sup> simplifies considerably, as described by Wald.<sup>9</sup> We cite the important results here.

Consider a set of  $n$  orthonormal vectors  $e_\mu$ ,

$$\sum_{i=1}^n (e_\mu)^i (e_\nu)_i = \delta_{\mu\nu}, \quad \sum_{\mu=1}^n (e_\mu)^i (e_\mu)_j = \delta^i_j, \quad (3.3)$$

where  $(e_\mu)^i$  and  $(e_\mu)_i$  are related by the metric via  $(e_\mu)_i = \sum_j g_{ij} (e_\mu)^j$ . In such a basis, the Ricci tensor is

$$R_{\mu\nu} = \sum_{i,\sigma} \nabla_i [(e_\sigma)^i \omega_{\mu\nu\sigma} - (e_\mu)^i \omega_{\sigma\nu\sigma}] + \sum_{\sigma,\tau} (\omega_{\sigma\nu\sigma} \omega_{\tau\tau\mu} - \omega_{\sigma\tau\mu} \omega_{\tau\nu\sigma}), \quad (3.4)$$

where the *Ricci rotation coefficients* are

$$\omega_{\sigma\mu\nu} := \sum_{i,j} (e_\sigma)^i (e_\mu)^j \nabla_i (e_\nu)_j. \quad (3.5)$$

We have that  $\omega_{\sigma\mu\nu} = -\omega_{\sigma\nu\mu}$ , so there are  $n^2(n-1)/2$  independent  $\omega$ 's (two in two dimensions, nine in three). The symbol  $\nabla_i$  denotes the covariant derivative with respect to the  $i$ th coordinate. For our purposes,  $\nabla_i$  can be taken to be an ordinary derivative,<sup>26</sup> except when it appears as a divergence, where an extra factor involving the determinant of the metric is required:

$$\sum_i \nabla_i V^i = \sum_i \frac{1}{\sqrt{g}} \frac{\partial}{\partial \xi^i} (\sqrt{g} V^i), \quad (3.6)$$

so for incompressible flows there is no practical difference.

The Ricci rotation coefficients carry information similar to the Christoffel symbols  $\Gamma$ , but are defined in terms of the orthonormal basis vectors  $\mathbf{e}_\mu$  instead of derivatives of the metric.

Summing over the indices of Eq. (3.4), we obtain the Ricci scalar,

$$R = \sum_\mu R_{\mu\mu} = 2 \sum_{i,j,\sigma} \nabla_i [(e_\sigma)^i \nabla_j (e_\sigma)^j] - \sum_{\sigma,\tau,\mu} (\omega_{\sigma\sigma\mu} \omega_{\tau\tau\mu} - \omega_{\sigma\tau\mu} \omega_{\tau\sigma\mu}), \quad (3.7)$$

where we have made use of the identity

$$\sum_\mu \omega_{\mu\mu\sigma} = \sum_i \nabla_i (e_\sigma)^i,$$

easily verified directly from the definition of  $\omega$ , Eq. (3.5). The Ricci tensor and scalar in an orthonormal frame, respectively Eqs. (3.4) and (3.7), are the quantities we use in Secs. IV and V to derive constraints on dynamical systems.

Equation (3.3) states that the vectors  $\mathbf{e}_\mu$  are orthonormal with respect to a metric. We want to use the metric given by Eq. (2.3), so we take

$$(e_\mu)_i = \Lambda_\mu^{1/2} (\hat{e}_\mu)_i, \quad (e_\mu)^i = \Lambda_\mu^{-1/2} (\hat{e}_\mu)^i, \quad (3.8)$$

where, because the underlying space is Euclidean, we have  $(\hat{e}_\mu)_i = (\hat{e}_\mu)^i$ . It is then clear that (3.3) is satisfied. The definitions (3.8) are called the covariant (subscripted) and contravariant (superscripted) representations of the vectors  $\mathbf{e}_\mu$ . For a chaotic system, this definition of  $\mathbf{e}_\mu$  implies that for long times the components  $(e_s)^i =: s^i$  and  $(e_u)_i =: u_i$  are growing exponentially, and  $(e_s)_i =: s_i$  and  $(e_u)^i =: u^i$  are decaying exponentially. It is these radically different time-asymptotic behaviors that allows the derivation of the constraints in Secs. IV and V.

#### IV. CONSTRAINTS ON TWO-DIMENSIONAL SYSTEMS

In Sec. III, we derived a form for the Ricci tensor expressed in a basis aligned with the characteristic directions  $\hat{\mathbf{e}}_\mu$  of the flow. As mentioned in Sec. III, the symmetries of



the Riemann curvature tensor imply that in two dimensions it has only one independent component, given by the Ricci scalar, Eq. (3.7). In two dimensions, the terms in the Ricci scalar quadratic in  $\omega$  cancel:

$$\sum_{\sigma,\tau,\mu} (\omega_{\sigma\sigma\mu} \omega_{\tau\tau\mu} - \omega_{\sigma\tau\mu} \omega_{\tau\sigma\mu}) = \omega_{221} \omega_{221} + \omega_{112} \omega_{112} - \omega_{221} \omega_{221} - \omega_{112} \omega_{112} = 0.$$

Hence, the Ricci scalar reduces to the simple form

$$R = 2 \sum_{i,j,\sigma=1}^2 \nabla_i [(e_\sigma)^i \nabla_j (e_\sigma)^j]. \quad (4.1)$$

As mentioned in Sec. II, we are assuming the underlying space is flat, so that  $R \equiv 0$  always. Equation (4.1) is essentially the same expression as derived in Ref. 1, but rewritten in a more transparent form and allowing for compressibility of the vector field  $\mathbf{v}(\mathbf{x}, t)$  (because here the derivatives  $\nabla_i$  are covariant). Notice that the Lyapunov exponents enter the Ricci scalar through the definition of  $(e_\sigma)^i$ , Eq. (3.8), as  $\Lambda_\sigma^{-1/2} = \exp(-\lambda_\sigma t)$ .

As a direct demonstration of the vanishing of the Ricci scalar for the nonchaotic case, let us take the flow  $\mathbf{v}(x_1, x_2) = (f(x_2), 0)$ , a shear flow of velocity  $f(x_2)$  along the  $x_1$  direction. For this special case, Eq. (2.1) can be explicitly solved, and the Lagrangian trajectories are given by

$$x_1 = \xi_1 + t f(\xi_2), \quad x_2 = \xi_2.$$

The corresponding metric tensor is

$$g_{ij} = \sum_\ell \frac{\partial x^\ell}{\partial \xi^i} \frac{\partial x^\ell}{\partial \xi^j} = \begin{pmatrix} 1 & t f'(\xi_2) \\ t f'(\xi_2) & 1 + t^2 f'(\xi_2)^2 \end{pmatrix}.$$

The eigenvalues and eigenvectors of  $g$  are then straightforward to calculate. Direct insertion into formula (4.1) for the Ricci scalar in two-dimensions confirms, after a tedious calculation, that it does indeed vanish identically. When the flow is not chaotic, the usefulness of Eq. (4.1) is thus somewhat limited: it is simply an identity that is always satisfied. At best, verification that the Ricci scalar vanishes is a somewhat complicated consistency check.

The real usefulness of Eq. (4.1) becomes more apparent when the Lagrangian trajectories are taken to be chaotic (which in two dimensions requires a time-dependent flow). It is still true that the Ricci scalar (4.1) vanishes identically, because the coordinate transformation  $\mathbf{x}(\boldsymbol{\xi}, t)$  is differentiable. However, there is information to be gained by considering what we call the *curvature balance*, that is, the details of how the vanishing of the curvature tensor is realized in the chaotic flow. We now proceed to examine this balance.

Let us write

$$\lambda_\mu(\boldsymbol{\xi}, t) = \lambda_\mu^\infty + \frac{\eta_\mu(\boldsymbol{\xi}, t)}{t}, \quad (4.2)$$

where the dimensionless function  $\eta_\mu(\boldsymbol{\xi}, t)$  satisfies  $\lim_{t \rightarrow \infty} \eta_\mu(\boldsymbol{\xi}, t)/t = 0$ . The choice of the factor of  $1/t$  is motivated by the form for the time-evolution of the Lyapunov exponents derived by Goldhirsch *et al.*<sup>5</sup> based on a direct analysis of the differential equations they

satisfy. Essentially,  $\eta_\mu(\boldsymbol{\xi}, t)$  is a “noise” term of relatively small amplitude: the dominant time-asymptotic behavior of the finite-time Lyapunov exponents is as  $1/t$ . Note that with this definition  $\nabla_i \lambda_\mu t = \nabla_i \eta_\mu$ .

Having posed the form (4.2) for the finite-time Lyapunov exponents, we can rewrite (4.1) as

$$R = 2 \sum_{i,j,\sigma=1}^2 e^{-2\lambda_\sigma^\infty t} \nabla_i \left[ e^{-\eta_\sigma} (\hat{e}_\sigma)^i \nabla_j (e^{-\eta_\sigma} (\hat{e}_\sigma)^j) \right]. \quad (4.3)$$

Now we can clearly see the asymptotic time dependence of each term for large  $t$ :

$$R = 2e^{-2|\lambda_u^\infty|t} \nabla_i \left[ e^{-\eta_u} \hat{u}^i \nabla_j (e^{-\eta_u} \hat{u}^j) \right] + 2e^{+2|\lambda_s^\infty|t} \nabla_i \left[ e^{-\eta_s} \hat{s}^i \nabla_j (e^{-\eta_s} \hat{s}^j) \right] \quad (4.4)$$

We have put absolute values around the exponents to exhibit the sign of the exponential, following our assumption that there is an expanding (positive) exponent,  $\lambda_u^\infty$ , and a contracting (negative) exponent,  $\lambda_s^\infty$ .

Since  $R$  vanishes identically, either the two terms in Eq. (4.4) both vanish identically (as is the case for purely hyperbolic systems such as Arnold’s cat map<sup>1</sup>), or they must balance each other, growing at the same exponential rate  $2\Delta$ :

$$R = 2e^{2\Delta t} \left\{ e^{-2(|\lambda_u^\infty|+\Delta)t} \nabla_i \left[ e^{-\eta_u} \hat{u}^i \nabla_j (e^{-\eta_u} \hat{u}^j) \right] + e^{+2(|\lambda_s^\infty|-\Delta)t} \nabla_i \left[ e^{-\eta_s} \hat{s}^i \nabla_j (e^{-\eta_s} \hat{s}^j) \right] \right\}. \quad (4.5)$$

In other words, the growth rate  $\Delta$  is defined by the requirement that each term inside the braces in Eq. (4.5) be of order one asymptotically. Thus, for large time we must have

$$\nabla_i \left[ e^{-\eta_u} \hat{u}^i \nabla_j (e^{-\eta_u} \hat{u}^j) \right] \sim \exp(+2(|\lambda_u^\infty| + \Delta)t), \quad (4.6)$$

$$\nabla_i \left[ e^{-\eta_s} \hat{s}^i \nabla_j (e^{-\eta_s} \hat{s}^j) \right] \sim \exp(-2(|\lambda_s^\infty| - \Delta)t). \quad (4.7)$$

These growth rates apply even if  $\sqrt{g}$  grows or decays exponentially in time, since because of Eq. (3.6) it appears both in the numerator and the denominator. If  $\Delta > |\lambda_s^\infty|$ , then both (4.6) and (4.7) *grow* exponentially. If  $\Delta < |\lambda_s^\infty|$ , for  $t \gg (|\lambda_s^\infty| - \Delta)^{-1}$  we have

$$\nabla_i \left[ e^{-\eta_s} \hat{s}^i \nabla_j (e^{-\eta_s} \hat{s}^j) \right] = 0 \quad (4.8)$$

to exponential accuracy in  $t$ . In practice, we have found only cases with  $-|\lambda_u^\infty| \leq \Delta < |\lambda_s^\infty|$ . Equation (4.8) is thus a differential constraint equation relating  $\hat{\mathbf{s}}$  and  $\eta_s$ .

Note that we do not have to wait for the Lyapunov exponent itself to have converged for the constraint (4.8) to be satisfied: it is sufficient that the quantity  $|\lambda_s| - \Delta$  have a definite sign, which occurs rapidly in practice.

Having derived Eq. (4.8), we now show that it can be reduced to a simpler constraint. Let

$$K := \nabla_i (e^{-\eta_s} \hat{s}^i). \quad (4.9)$$

The constraint Eq. (4.8) can be written

$$\frac{dK}{d\bar{\tau}} = -K^2, \quad \frac{d}{d\bar{\tau}} := e^{-\eta_s} \hat{s}^i \nabla_i, \quad (4.10)$$

where  $\bar{\tau}$  is a parameter that measures the distance along an  $\hat{\mathbf{s}}$ -line, weighed by a density of  $\exp(-\eta_s)$  [this relation is well-defined because  $\exp(-\eta_s) > 0$ ]. The ordinary differential equation (4.10) has solution

$$K = \frac{K_0}{1 + (\bar{\tau} - \bar{\tau}_0)K_0}, \quad (4.11)$$

which has a singularity at  $\bar{\tau} - \bar{\tau}_0 = -K_0^{-1}$ . Since all the quantities that make up  $K$  are well-defined for a given point on the  $\hat{\mathbf{s}}$ -line, we have to reject the nonvanishing solution to Eq. (4.10), and instead take  $K \equiv 0$ . Hence, the constraint

$$\nabla_i (e^{-\eta_s} \hat{s}^i) = 0 \quad (4.12)$$

is necessary and sufficient for Eq. (4.8) to be satisfied. Equation (4.12) can also be written

$$\nabla_i \hat{s}^i - \hat{s}^i \nabla_i \eta_s = 0. \quad (4.13)$$

This is a compressible version of the constraint that was obtained in Ref. 1. If we use  $\ln \sqrt{g} = \lambda_u t + \lambda_s t$ , we can rewrite (4.13) as

$$\nabla \cdot \hat{\mathbf{s}} + \hat{\mathbf{s}} \cdot \nabla \lambda_u t = 0, \quad (4.14)$$

where the  $\nabla$  are ordinary derivatives (*i.e.*, non-covariant) and any direct reference to compressibility effects drops out, but the constraint now takes the form of a relation between the stable direction,  $\hat{\mathbf{s}}$ , and the unstable stretching rate,  $\lambda_u$ .

To illustrate the result, we use the oscillating convection rolls system, Eq. (2.7). We consider the  $\hat{\mathbf{s}}$ -line starting at  $A$  and ending at  $B$  in Fig. 1, with the same parameter values. In Fig. 3 we plot the two terms of Eq. (4.14) along that line for different times; it is clear that their sum converges rapidly to zero. Figure 3 highlights another property of the constraint (4.13): if  $\lim_{t \rightarrow \infty} \nabla_i \hat{s}^i$  exists (which it does in every case under consideration here), so must  $\lim_{t \rightarrow \infty} \hat{s}^i \nabla_i \eta_s$ .

To exhibit the rate of exponential convergence to zero of Eq. (4.14), we consider the flow

$$\dot{x}^1 = x^2 + \sin x^1 \sin x^2, \quad \dot{x}^2 = \mu x^1 + \nu x^2 + \cos x^1 \cos x^2. \quad (4.15)$$

This is a two-dimensional autonomous system, so it cannot formally exhibit chaos. Nevertheless, for adequate choice of  $\mu$  and  $\nu$  trajectories of (4.15) grow exponentially away from the origin, so that Lyapunov exponents are well-defined even though they are not tied to any chaos in the system. One could also achieve such nonzero exponents with a linear system, but then the  $\hat{\mathbf{u}}$ - and  $\hat{\mathbf{s}}$ -lines would be straight, with vanishing derivatives, so that Eq. (4.14) is satisfied trivially. The nonlinear terms in in (4.15) do not contribute to  $\nabla \cdot \mathbf{v} = \nu$ . Figure 4 shows the evolution of  $\nabla \cdot \hat{\mathbf{s}} + \hat{\mathbf{s}} \cdot \nabla \lambda_u t$  for parameter values  $\mu = 1$ ,  $\nu = -1$ . The convergence rate is found to be  $-(\lambda_u + |\lambda_s|)$ , corresponding to  $\Delta = -\lambda_u$  in Eq. (4.7). This implies from Eq. (4.6) that  $\nabla_i (\exp(-\eta_u) \hat{u}^i)$  remains of order one, as confirmed by numerical

calculation (Fig. 4, bottom). In truly chaotic systems, the convergence rate is not so readily obtained because the coefficient of the exponential has large fluctuations.

The rate of convergence of the nonchaotic system seems to be an extreme case. The derivatives of the Lyapunov exponents along the unstable direction are well-behaved and do not grow exponentially, so from Eq. (4.6) we must have  $\Delta = -\lambda_u$ . This leads to an extremely fast convergence rate for the constraint (4.14). For chaotic systems, we find the derivatives of the Lyapunov exponents along the unstable direction grow exponentially, so the convergence rate of the constraint is slower (but still quite fast).

The numerical evaluation of the Lagrangian derivatives of  $\lambda_\mu(\boldsymbol{\xi}, t)$  and  $\mathbf{e}_\mu(\boldsymbol{\xi}, t)$  is not straightforward. Finite-differencing (by starting two trajectories very close to each other) does not work well because of potentially very steep variations along the unstable direction. Also, it is difficult to guarantee that the two trajectories are in the same chaotic region when they are very close to region boundaries. A better method is to take the Lagrangian derivative of the set of equations used to find the Lyapunov exponents and eigenvectors themselves, which yields a set of ordinary differential equations for those derivatives. This is related to the method used by Tang and Boozer,<sup>1</sup> who used the Lagrangian derivative of the linearized system (2.6) directly. The method is unstable, but since the quantities under consideration converge quickly (the Lyapunov exponents are not sought, only their derivatives), reasonable accuracy can be achieved. In this paper, we have used a differentiated version of the continuous Gram–Schmidt orthonormalization method of Goldhirsch *et al.*<sup>5</sup> with a stabilizing factor.<sup>18,19</sup> The method of Goldhirsch *et al.* was derived independently by Greene and Kim,<sup>4</sup> including the stabilizing factor.

## V. CONSTRAINTS ON THREE-DIMENSIONAL SYSTEMS

In three spatial dimensions, the six independent components of the Riemann curvature tensor are embodied in the Ricci tensor (see Sec. III). As opposed to the two-dimensional case, the terms quadratic in the  $\omega$ 's in the Ricci tensor, Eq. (3.4), do not vanish.

The three diagonal elements of the Ricci tensor can be written as

$$R_{\tau\tau} = \nabla_i \left[ (e_\tau)^i (\mathcal{H}_{\nu\mu} - \mathcal{H}_{\mu\nu}) + (e_\nu)^i \mathcal{H}_{\mu\tau} - (e_\mu)^i \mathcal{H}_{\nu\tau} \right] + 2\mathcal{H}_{\mu\nu} \mathcal{H}_{\nu\mu} + \frac{1}{2} \left[ (\mathcal{H}_{\mu\mu} - \mathcal{H}_{\nu\nu})^2 - \mathcal{H}_{\tau\tau}^2 \right] \quad (5.1)$$

and the three off-diagonal elements as

$$R_{\mu\nu} = \nabla_i \left[ (e_\nu)^i \mathcal{H}_{\nu\tau} - (e_\mu)^i \mathcal{H}_{\mu\tau} + (e_\tau)^i (\mathcal{H}_{\mu\mu} - \mathcal{H}_{\nu\nu}) \right] + \mathcal{H}_{\tau\mu} \mathcal{H}_{\nu\tau} + \mathcal{H}_{\tau\nu} \mathcal{H}_{\mu\tau} + (\mathcal{H}_{\mu\nu} + \mathcal{H}_{\nu\mu})(\mathcal{H}_{\mu\mu} + \mathcal{H}_{\nu\nu} - \mathcal{H}_{\tau\tau}), \quad (5.2)$$

where  $(\mu, \nu, \tau)$  are ordered cyclically (*i.e.*,  $(\mu, \nu, \tau) = \{(u, m, s), (m, s, u), (s, u, m)\}$ ) and the *characteristic helicities* are defined as

$$\mathcal{H}_{\mu\nu} := \frac{1}{\sqrt{g}} (e_\mu)_i \varepsilon^{ijk} \nabla_j (e_\nu)_k.$$

The main result of this section is as follows: if all the terms in Eq. (5.1) are bounded from above by  $\exp(2|\lambda_s^\infty|t)$ , then the constraints

$$\hat{\mathbf{u}} \cdot \nabla \times \hat{\mathbf{m}} - \hat{\mathbf{s}} \cdot \nabla \lambda_m t = 0, \quad (5.3)$$

$$\hat{\mathbf{m}} \cdot \nabla \times \hat{\mathbf{u}} + \hat{\mathbf{s}} \cdot \nabla \lambda_u t = 0, \quad (5.4)$$

$$\hat{\mathbf{u}} \cdot \nabla \times \hat{\mathbf{u}} = 0, \quad (5.5)$$

hold to exponential accuracy for large times. Taking the difference between (5.4) and (5.3) and using vector identities yields

$$\frac{1}{\sqrt{g}} \nabla \cdot (\sqrt{g} \hat{\mathbf{s}}) - \hat{\mathbf{s}} \cdot \nabla \lambda_s t \longrightarrow 0, \quad (5.6)$$

the same constraint as for the two-dimensional case, Eq. (4.13). The constraint (5.6) was observed numerically for three-dimensional volume-preserving maps by Tang and Boozer.<sup>2</sup> We thus see that Eq. (5.6) is a consequence of two new, separate constraints. The third constraint, Eq. (5.5), is different in nature than the previous ones, since it involves no Lyapunov exponents.

If we “lift” a two-dimensional system to three dimensions by simply adding a third dimension corresponding to  $\hat{\mathbf{m}} = \hat{\mathbf{s}} \times \hat{\mathbf{u}} = \text{constant}$ , the constraint (5.3) is satisfied trivially because  $\lambda_m = 0$  and  $\hat{\mathbf{m}}$  is independent of position. The constraint (5.4) can be equated to (4.13), the two-dimensional constraint, and (5.5) is trivially satisfied because  $\nabla \times \hat{\mathbf{u}}$  is in the  $\hat{\mathbf{m}}$  direction. Thus, as required for consistency, we recover the two-dimensional constraint from the three-dimensional ones.

We now proceed with the derivation of the constraints (5.3)–(5.4). The argument is similar to the two-dimensional case, but is complicated by the possibility that the terms in Eq. (5.1) and (5.2) grow at different rates, since there are more than two terms in the expression. There are also six independent components to the Ricci tensor, as opposed to just one in the two-dimensional case.

Define

$$\tilde{\mathcal{H}}_{\mu\nu} := (\hat{e}_\mu)_i \varepsilon^{ijk} \nabla_j (\hat{e}_\nu)_k - \sum_\tau \varepsilon_{\mu\nu\tau} (\hat{e}_\tau)^j \nabla_j \eta_\nu \quad (5.7)$$

where  $\eta_\nu$  is defined in (4.2), so that  $\mathcal{H}_{\mu\mu} = (\Lambda_\mu/\sqrt{g}) \tilde{\mathcal{H}}_{\mu\mu}$  and  $\mathcal{H}_{\mu\nu} = \Lambda_\tau^{-1/2} \tilde{\mathcal{H}}_{\mu\nu}$ ,  $\mu \neq \nu$ . With this definition we have separated the long-time behavior of  $\mathcal{H}_{\mu\nu}$  that is due to the infinite-time Lyapunov exponents.

We focus first on the diagonal components, given by Eq. (5.1). Let  $2\Delta_{\tau\tau}$  be the asymptotic growth rate of the fastest-growing term (or terms) in (5.1). (In two dimensions, there was only one common growth rate  $\Delta$  for the two terms in  $R$ , since they had to cancel.) Factoring out  $\exp(2\Delta_{\tau\tau}t)$  from Eq. (5.1), we obtain

$$\begin{aligned} R_{\tau\tau} = & e^{2\Delta_{\tau\tau}t} \left\{ \nabla_i \left[ e^{-2(\lambda_\tau + \Delta_{\tau\tau})t} (\hat{e}_\tau)^i (\tilde{\mathcal{H}}_{\nu\mu} - \tilde{\mathcal{H}}_{\mu\nu}) + e^{-2(\lambda_\nu + \Delta_{\tau\tau})t} (\hat{e}_\nu)^i \tilde{\mathcal{H}}_{\mu\tau} \right. \right. \\ & \left. \left. - e^{-2(\lambda_\mu + \Delta_{\tau\tau})t} (\hat{e}_\mu)^i \tilde{\mathcal{H}}_{\nu\tau} \right] + 2e^{-2(\lambda_\tau + \Delta_{\tau\tau})t} \tilde{\mathcal{H}}_{\mu\nu} \tilde{\mathcal{H}}_{\nu\mu} \right. \\ & \left. + \frac{1}{2} \left[ \left( e^{-(\lambda_\nu + \lambda_\tau - \lambda_\mu + \Delta_{\tau\tau})t} \tilde{\mathcal{H}}_{\mu\mu} - e^{-(\lambda_\mu + \lambda_\tau - \lambda_\nu + \Delta_{\tau\tau})t} \tilde{\mathcal{H}}_{\nu\nu} \right)^2 - e^{-2(\lambda_\mu + \lambda_\nu - \lambda_\tau + \Delta_{\tau\tau})t} \tilde{\mathcal{H}}_{\tau\tau}^2 \right] \right\}, \quad (5.8) \end{aligned}$$

where, by the definition of  $\Delta_{\tau\tau}$ , all the terms inside the braces are asymptotically either of order one or decreasing exponentially in time. We are interested in the terms that have a positive growth rate in the exponential; for such terms to remain of order one or less the coefficient of the exponential has to go to zero exponentially, as was the case in two dimensions.

In each  $R_{\tau\tau}$  there is a term with coefficient  $\exp(-2(\lambda_s^\infty + \Delta_{\tau\tau})t)$ : if  $\Delta_{\tau\tau} < |\lambda_s^\infty|$  then that coefficient grows exponentially at a rate  $\exp(2(|\lambda_s^\infty| - \Delta_{\tau\tau})t)$ . This implies that the coefficient of the exponential decreases at least as fast as  $\exp(-2(|\lambda_s^\infty| - \Delta_{\tau\tau})t)$ . Thus, from each diagonal components  $R_{\tau\tau}$ , we get

$$\nabla_i \left[ e^{-2\eta_s \hat{s}^i} \tilde{\mathcal{H}}_{mu} \right] < \exp(-2(|\lambda_s^\infty| - \Delta_{uu})t), \quad \text{from } R_{uu}; \quad (5.9)$$

$$\nabla_i \left[ e^{-2\eta_s \hat{s}^i} \tilde{\mathcal{H}}_{um} \right] < \exp(-2(|\lambda_s^\infty| - \Delta_{mm})t), \quad \text{from } R_{mm}; \quad (5.10)$$

$$\nabla_i \left[ e^{-2\eta_s \hat{s}^i} (\tilde{\mathcal{H}}_{mu} - \tilde{\mathcal{H}}_{um}) \right] + 2\tilde{\mathcal{H}}_{mu} \tilde{\mathcal{H}}_{um} < \exp(-2(|\lambda_s^\infty| - \Delta_{ss})t), \quad \text{from } R_{ss}; \quad (5.11)$$

The two constraints (5.9) and (5.10) can be directly inserted into (5.11), which then says that the product  $\tilde{\mathcal{H}}_{mu} \tilde{\mathcal{H}}_{um}$  decreases exponentially to zero. Since

$$\tilde{\mathcal{H}}_{mu} - \tilde{\mathcal{H}}_{um} = e^{\eta_s} K,$$

where  $K$  is defined in (4.9), we can use the argument, proved in the two-dimensional case, that if  $\nabla_i[s^i K] = 0$ , then  $K = 0$ . Thus,  $\tilde{\mathcal{H}}_{mu} = \tilde{\mathcal{H}}_{um}$ , and their product goes to zero, so both  $\tilde{\mathcal{H}}_{mu}$  and  $\tilde{\mathcal{H}}_{um}$  must go to zero. From the definition (5.7), we see that we have just demonstrated the constraints (5.3) and (5.4), with the assumption that  $\Delta_{\tau\tau} < |\lambda_s^\infty|$ .

Also, in each  $R_{\tau\tau}$  there is a term with coefficient  $\exp(2(\lambda_u^\infty - \lambda_m^\infty - \lambda_s^\infty - \Delta_{\tau\tau})t)$ . Since  $\lambda_u^\infty > \lambda_m^\infty$ , the condition  $\Delta < |\lambda_s^\infty|$  is sufficient for the growth rate to be positive. This leads directly to

$$\tilde{\mathcal{H}}_{uu} < \exp(-(\lambda_u^\infty - \lambda_m^\infty + |\lambda_s^\infty| - \Delta_{\tau\tau})t),$$

which proves the last constraint, Eq. (5.5).

There could be other constraints, depending on the relative magnitude of the Lyapunov exponents and the sign of  $\lambda_m^\infty$ . However, the constraints derived here have the broadest applicability and are expected to be true in general. The requirement that  $\Delta < |\lambda_s^\infty|$  has been found to hold by a wide margin for every dynamical system that we have tested. Given that the Lyapunov exponents enter the Ricci tensor through  $\Lambda_\mu^{-1}$ , so that the largest growth rate is  $2|\lambda_s^\infty|$ , it is reasonable to assume that the terms in the Ricci scalar could grow no faster than the timescale  $2\Delta = 2|\lambda_s^\infty|$ .

To exhibit the convergence of these quantities, we use the model system

$$\dot{x}^1 = x^2 + \sin x^1 \sin x^2 \sin x^3, \quad \dot{x}^2 = x^3 + \cos x^1 \cos x^2 \sin x^3, \quad \dot{x}^3 = \lambda x^1 + \mu x^2 + \nu x^3. \quad (5.12)$$

These are an extension of the two-dimensional nonchaotic equations (4.15) presented earlier. In the three-dimensional case, the system is generically chaotic, but can have unbounded trajectories for certain parameter values. If we pick an initial condition near the origin, then

initially the nonlinear terms are important, but become less so as the trajectory gets further away. Thus, Eqs. (5.12) have nontrivial characteristic manifolds near the origin but have a time-asymptotic form that is well-behaved (linear exponential growth). Figures 5 and 6 show the convergence of (5.3) and (5.4) for different parameter values, one set incompressible ( $\nu = 0$ ) and the other compressible ( $\nu \neq 0$ ); Figures 7 and 8 show the convergence of (5.5) for the same parameter values. For this simple system, the rate of convergence for all the constraints is found to be  $-2(\lambda_u - \lambda_m)$ .

A more practical example is the *ABC* flow,

$$\mathbf{v}(\mathbf{x}) = A(0, \sin x^1, \cos x^1) + B(\cos x^2, 0, \sin x^2) + C(\sin x^3, \cos x^3, 0) \quad (5.13)$$

a sum of three Beltrami waves which satisfy  $\nabla \times \mathbf{v} \propto \mathbf{v}$ . This flow is time-independent, incompressible ( $g = 1$ ), and is well-studied in the context of dynamo theory; we use the parameter values  $A = 5, B = C = 2$ , which are known to exhibit a vigorous dynamo.<sup>11,27</sup> (All the results presented here also apply to the more common  $A = B = C = 1$  flow, though the convergence rate of the constraints is slower because that flow is less chaotic.) Figure 9 shows the convergence of the two terms of (5.3) and (5.4); they are seen to track each other as time evolves. Figure 10 is a logarithmic plot of  $\tilde{\mathcal{H}}_{um}$  and  $\tilde{\mathcal{H}}_{mu}$  as a function of time, showing that the two quantities have converged to order  $10^{-7}$ . The convergence is not linear: it exhibits large fluctuations, yet the decreasing trend is evident.

Finally, no demonstration of a method would be complete without applying it to the celebrated Lorenz model,<sup>12</sup>

$$\dot{x}^1 = \sigma(x^2 - x^1), \quad \dot{x}^2 = r x^1 - x^2 - x^1 x^3, \quad \dot{x}^3 = -b x^3 + x^1 x^2, \quad (5.14)$$

which is a compressible vector field with  $\nabla \cdot \mathbf{v} = -(\sigma + 1 + b)$ . We use Lorenz's parameter values of  $\sigma = 10, b = 8/3, r = 28$ . The initial condition we used is  $\boldsymbol{\xi} = (0, 1, 0)$ , which has a trajectory that initially skirts an unstable fixed point and undergoes nearly-periodic oscillations around it. Thus, the convergence of the constraints is momentarily delayed until the trajectory can explore the attractor, which is seen to happen at  $t \simeq 20$  in Figures 12–14. Note that this does not mean that if the trajectory comes near a fixed point again the convergence to zero will be undone: it will pause momentarily, to resume after the trajectory leaves the vicinity of the fixed point.

The off-diagonal terms (5.2) involve the same quantities as the diagonal ones, so they do not immediately yield any new constraints. However, they may be useful in trying to establish a detailed curvature balance for the Ricci tensor (see below).

It should be noted in closing this section that for the three-dimensional case we have not made use of the fact that the curvature actually *vanishes*. We have simply assumed that its individual terms grow no faster than  $\exp(2|\lambda_s|t)$ . In contrast to the two-dimensional case, we have made no detailed assessment of the balance of curvature, a difficult task because of the number of terms involved. However, hints of this balance can often be seen in the numerical results, such as when  $\tilde{\mathcal{H}}_{um}$  and  $\tilde{\mathcal{H}}_{mu}$  track each other precisely in Figs. 6 and 13, or in Fig. 11, where  $\tilde{\mathcal{H}}_{mm}$  and  $\tilde{\mathcal{H}}_{ss}$  also track each other exactly.

## VI. DISCUSSION

Using the requirement that, in a flat space, the Riemannian curvature must vanish in any coordinate system, we have derived the constraints (4.13) in two dimensions, a generalization of the work of Tang and Boozer<sup>1</sup> to compressible flows, with a more detailed examination of the underlying assumptions. We have also verified the constraint for flows, whereas previous work had focused on area-preserving maps. Equation (4.13) is a constraint relating the stable direction,  $\hat{\mathbf{s}}$ , and the finite-time Lyapunov exponent,  $\lambda_s$ ; it is satisfied to exponential accuracy in time in a chaotic flow.

With the same assumptions as in two dimensions, we have derived the same constraint in three dimensions, Eq. (5.6), verifying the conjecture of Tang and Boozer<sup>2</sup> inspired by numerical results on volume-preserving maps. In three dimensions, it is a consequence of two separate constraints, Eqs. (5.3) and (5.4). There is also a third constraint, Eq. (5.5), involving only the unstable direction,  $\hat{\mathbf{u}}$ , and no finite-time Lyapunov exponents. All have been shown numerically to hold with exponential accuracy in time for *ABC* flow and the Lorenz model, and we have verified the constraint for several other flows and maps, parameter values, and initial conditions. Two of the three-dimensional constraints are satisfied trivially in two dimensions, and the third is just the two-dimensional constraint (4.13), showing the consistency of the results.

The constraint (5.6) actually applies in any number of dimensions, as long as the usual assumption holds: all the terms in the Ricci scalar (3.7) must be bounded from above by  $\exp(2|\lambda_s|t)$ . There is then a  $\nabla_i[s^i \nabla_j s^j]$  term in the Ricci scalar that yields the constraint (5.6). The higher-dimensional generalization of Eqs. (5.3), (5.4), and (5.5) involve Lie brackets instead of curls, and a detailed analysis of their form remains to be done.

Though the constraints are interesting from the mathematical standpoint, it is natural to ask the following: what physical impact do the constraints have? Previous work has focussed on the constraint (5.6) in two<sup>1,7</sup> and three<sup>2,28</sup> dimensions. We review this work and discuss the consequences of the new, three-dimensional constraints.

In Ref. 1, it was found that the advection-diffusion equation in Lagrangian coordinates is a diffusion equation with an anisotropic diffusion tensor  $D^{ij} = D g^{ij}$ , where  $D$  is the scalar molecular diffusivity and  $g^{ij}$  is the inverse of the metric tensor given by Eq. (2.2). The dominant direction of diffusion is along the  $\hat{\mathbf{s}}$  line, with  $\hat{s}_i D^{ij} \hat{s}_j = D \exp(-2\lambda_s t)$ , which grows exponentially because  $\lambda_s < 0$ . In contrast, the diffusion along the  $\hat{\mathbf{u}}$  line is exponentially damped at a rate  $\exp(-2\lambda_u t)$ . Thus, after a short time essentially all the diffusion occurs along the  $\hat{\mathbf{s}}$  line. This counterintuitive result is a consequence of the diffusion equation smoothing out strong gradients, which are being created along the  $\hat{\mathbf{s}}$  line because of the *contraction* of fluid elements along that direction. Thus, it is the stable direction and  $\lambda_s$ —and not  $\lambda_u$ —that characterize the chaotic enhancement to diffusion. This is where the constraint comes in: in Ref. 1 it was shown that, in two dimensions, Eq. (4.13) can be written

$$\hat{\mathbf{s}} \cdot \nabla(\lambda_s t - \ln \|\boldsymbol{\kappa}\|) + \hat{\mathbf{s}} \cdot (\boldsymbol{\kappa} \times \nabla \times \boldsymbol{\kappa}) / \|\boldsymbol{\kappa}\|^2 = 0,$$

where  $\boldsymbol{\kappa} = (\hat{\mathbf{s}} \cdot \nabla)\hat{\mathbf{s}}$  is the curvature of the  $\hat{\mathbf{s}}$  line (unrelated to the Riemannian curvature of the space). This implies that, along an  $\hat{\mathbf{s}}$  line, the variations in  $\lambda_s$  are related to the variations in  $\|\boldsymbol{\kappa}\|$ . Indeed, this is confirmed by calculations using maps in two<sup>1</sup> and three<sup>2</sup> dimensions: regions of the  $\hat{\mathbf{s}}$  line with large curvature have locally small Lyapunov exponents. We have



performed a similar calculation on the oscillating convection rolls system to demonstrate this correlation: Figure 15 (top) shows the magnitude of the curvature  $\kappa$  as a function of the distance along the  $\hat{\mathbf{s}}$  line labeled  $A$  to  $B$  in Fig. 1, parametrized by  $\tau$ . The bottom part of Fig. 15 is a plot of the instantaneous Lyapunov exponent  $\lambda = |\lambda_s|$  (the flow is incompressible, so the two exponents differ only by a sign) as a function of  $\tau$ . Notice the local minima in  $\lambda$  whenever the curvature is maximal. These locally small values of the Lyapunov exponent hinder the enhancement of diffusion in those regions. Such considerations were used to provide design criteria for a chemical reactor in Ref. 7. Numerically, the correlation was also verified for three-dimensional volume-preserving maps in Ref. 2.

The constraint (4.13) has also been used in the study of the dynamo problem,<sup>28</sup> where a magnetic field is embedded in a conducting chaotic flow. Boozer<sup>29</sup> and Boozer and Tang<sup>28</sup> have derived criteria that determine the spatial distribution of the magnetic field in terms of the magnitudes of the Lyapunov exponents.

The constraint on the unstable direction  $\hat{\mathbf{u}}$ , Eq. (5.5), potentially modifies these results. In Refs. 28 and 29, an asymptotic expression for the magnitude of the induced current in Lagrangian coordinates was derived,

$$j^2 \sim \Lambda_u^3 \{(\mathbf{B} \cdot \hat{\mathbf{u}}) \hat{\mathbf{u}} \cdot \nabla \times \hat{\mathbf{u}}\}^2 + O(\Lambda_u^2 \Lambda_m), \quad (6.1)$$

where  $\mathbf{B}$  is the magnetic field, and only the fastest-growing term, proportional to  $\Lambda_u^3$ , was kept. The assumption was that there was nothing special about  $\hat{\mathbf{u}} \cdot \nabla \times \hat{\mathbf{u}}$ , so it should be roughly of order one. However, we have found that typically  $\hat{\mathbf{u}} \cdot \nabla \times \hat{\mathbf{u}} \sim \Lambda_u^{-1} \Lambda_m \rightarrow 0$  (see Figures 7, 8, 11, and 14). Thus, the first term in Eq. (6.1) is actually of lower order than the neglected term: for a nonideal plasma with resistivity  $\eta$ , the power  $\eta j^2$  needed to sustain the dynamo is potentially much smaller than previously thought. The constraint (5.5) also modifies the growth rate of other quantities, such as the parallel current  $\mathbf{j} \cdot \mathbf{B}$ . A more detailed analysis remains to be done, where the constraints (5.3) and (5.4) might be found useful.

## ACKNOWLEDGMENTS

The authors thank Diego del-Castillo-Negrete for helpful suggestions. This work was supported by the National Science Foundation and the Department of Energy under a Partnership in Basic Plasma Science grant, No. DE-FG02-97ER54441.

## REFERENCES

- <sup>1</sup> X. Z. Tang and A. H. Boozer, “Finite time Lyapunov exponent and advection-diffusion equation,” *Physica D* **95**, 283 (1996).
- <sup>2</sup> X. Z. Tang and A. H. Boozer, “A Lagrangian analysis of advection-diffusion equation for a three dimensional chaotic flow,” *Phys. Fluids* **11**, 1418 (1999).
- <sup>3</sup> V. I. Oseledec, “A multiplicative theorem: Lyapunov characteristic numbers for dynamical systems,” *Trans. Moscow Math. Soc.* **19**, 197 (1968).
- <sup>4</sup> J. M. Greene and J. S. Kim, “The calculation of Lyapunov spectra,” *Physica D* **24**, 213 (1987).
- <sup>5</sup> I. Goldhirsch, P. Sulem, and S. A. Orszag, “Stability and Lyapunov stability of dynamical systems: A differential approach and a numerical method,” *Physica D* **27**, 311 (1987).
- <sup>6</sup> H. Aref, “Stirring by chaotic advection,” *J. Fluid Mech.* **143**, 1 (1984).
- <sup>7</sup> X. Z. Tang and A. H. Boozer, “Design criteria of a chemical reactor based on a chaotic flow,” *Chaos* **9**, 183 (1999).
- <sup>8</sup> This is true for any tensor, but only the Riemann tensor has the property that it vanishes for flat spaces.
- <sup>9</sup> R. M. Wald, *General Relativity* (University of Chicago Press, Chicago, 1984).
- <sup>10</sup> T. H. Solomon and J. P. Gollub, “Chaotic particle transport in time-dependent Rayleigh–Bénard convection,” *Phys. Rev. A* **38**, 6280 (1988).
- <sup>11</sup> S. Childress and A. D. Gilbert, *Stretch, Twist, Fold: The Fast Dynamo* (Springer-Verlag, Berlin, 1995).
- <sup>12</sup> E. N. Lorenz, “Deterministic nonperiodic flow,” *J. Atmos. Sci.* **20**, 130 (1963).
- <sup>13</sup> The Lyapunov exponents are independent of position for a given ergodic region, but there may be several regions, with different values for the infinite-time Lyapunov exponents. See for example Ref. 14.
- <sup>14</sup> J. Eckmann and D. Ruelle, “Ergodic theory of chaos and strange attractors,” *Rev. Modern Phys.* **57**, 617 (1985).
- <sup>15</sup> G. Benettin, L. Galgani, and J. M. Strelcyn, “Kolmogorov entropy and numerical experiments,” *Phys. Rev. A* **14**, 2338 (1976).
- <sup>16</sup> I. Shimada and T. Nagashima, “A numerical approach to ergodic problem of dissipative dynamical systems,” *Prog. Theoret. Phys.* **61**, 1605 (1979).
- <sup>17</sup> T. M. Janaki, G. Rangarajan, S. Habib, and R. D. Ryne, “Computation of the Lyapunov spectrum for continuous-time dynamical systems and discrete maps,” *Phys. Rev. E* **60**, 6614 (1999).
- <sup>18</sup> F. Christiansen and H. H. Rugh, “Computing Lyapunov spectra with continuous Gram–Schmidt orthonormalization,” *Nonlinearity* **10**, 1063 (1997).
- <sup>19</sup> J.-L. Thiffeault, “Lagrangian Derivatives in Chaotic Flows,” *Nonlinearity*, in submission (2001).
- <sup>20</sup> S. Wiggins, *Chaotic Transport in Dynamical Systems* (Springer-Verlag, New York, 1991).
- <sup>21</sup> M. Giona, A. Adrover, F. J. Muzzio, and S. Cerbelli, “The geometry of mixing in time-periodic chaotic flows. I. Asymptotic directionality in physically realizable flows and global invariant properties,” *Physica D* **132**, 298 (1999).
- <sup>22</sup> S. Cerbelli, J. M. Zalc, and F. J. Muzzio, “The evolution of material field lines curvature in deterministic chaotic flows,” *Chem. Eng. Sci.* **55**, 363 (2000).
- <sup>23</sup> B. Schutz, *Differential Geometry* (Cambridge University Press, Cambridge, U.K., 1980).

<sup>24</sup> S. Weinberg, *Gravitation and Cosmology: Principles and Applications of the General Theory of Relativity* (John Wiley & Sons, New York, 1972).

<sup>25</sup> An orthonormal basis is generally not a coordinate basis, *i.e.*, it does not correspond to vectors  $\{\partial/\partial x'^i\}$  induced by some coordinate transformation  $x'^i = f^i(\mathbf{x})$ .

<sup>26</sup> The derivatives in the definition of  $\omega$ , Eq. (3.5), must be covariant, but we shall not make direct use of that definition. A straightforward way to evaluate  $\omega$  is to write it as<sup>9</sup>

$$\omega_{\lambda\mu\nu} = \frac{1}{2} \left\{ (e_\mu)_i [e_\lambda, e_\nu]^i - (e_\nu)_i [e_\lambda, e_\mu]^i + (e_\lambda)_i [e_\mu, e_\nu]^i \right\},$$

where the Lie bracket in terms of ordinary partial derivatives is  $[v, w]^i = v^k \partial w^i / \partial \xi^k - w^k \partial v^i / \partial \xi^k$ .

<sup>27</sup> D. J. Galloway and U. Frisch, “Dynamo action in a family of flows with chaotic streamlines,” *Geophys. Astrophys. Fluid Dynamics* **36**, 53 (1986).

<sup>28</sup> X. Z. Tang and A. H. Boozer, “Anisotropies in magnetic field evolution and local Lyapunov exponents,” *Phys. Plasmas* **7**, 1113 (2000).

<sup>29</sup> A. H. Boozer, “Dissipation of magnetic energy in the solar corona,” *Astrophys. J.* **394**, 357 (1992).

## FIGURES

FIG. 1. The field of characteristic directions  $\hat{\mathbf{s}}^\infty$  for oscillating rolls, Eq. (2.7), with  $A = k = \epsilon = \omega = 1$ . Two typical portions of the stable manifold are shown.

FIG. 2. Typical portion of a stable manifold, or  $\hat{\mathbf{s}}^\infty$ -line, for the  $ABC$  flow with  $A = 5$ ,  $B = C = 2$ . The domain is  $2\pi$ -periodic in all three directions, as delimited by the dashed lines.

FIG. 3. For the system of oscillating convection rolls, Eq. (2.7), the convergence of the constraint  $\nabla \cdot \hat{\mathbf{s}} + (\hat{\mathbf{s}} \cdot \nabla)\lambda_u t \rightarrow 0$  is illustrated by evaluating its two terms on an  $\hat{\mathbf{s}}^\infty$ -line. Here  $\tau$  is the distance along the  $\hat{\mathbf{s}}^\infty$ -line from  $A$  to  $B$  in Fig. 1, the solid line is  $-\nabla \cdot \hat{\mathbf{s}}^\infty$ , and the dashed line is  $(\hat{\mathbf{s}}^\infty \cdot \nabla)\lambda_u t$ . Some parts of the line converge more slowly because the finite-time Lyapunov exponent is smaller in those regions (see Fig. 15).

FIG. 4. Top graph: Illustration of the exponential convergence of  $\nabla \cdot \hat{\mathbf{s}} + \hat{\mathbf{s}} \cdot \nabla \lambda_u t$ , for the nonchaotic two-dimensional model given by Eq. (4.15). The parameter values  $\mu = 1$  and  $\nu = -1$  are chosen such that the trajectories are exponentially diverging (the initial conditions are  $\boldsymbol{\xi} = (0.01, 0.015)$ ). The dashed line denotes an exponential with decay rate  $-(\lambda_u + |\lambda_s|) \simeq -(1.618 + 0.618) = -2.236$ . Bottom graph: plot of  $\nabla \cdot \hat{\mathbf{u}} + \hat{\mathbf{u}} \cdot \nabla \lambda_s t$ , showing that asymptotically it remains of order one.  $\nabla \cdot \hat{\mathbf{u}}$  actually converges to a nonzero constant; the oscillations are due to  $\hat{\mathbf{u}} \cdot \nabla \lambda_s t$ .

FIG. 5.  $\tilde{\mathcal{H}}_{um}$  (solid line) and  $\tilde{\mathcal{H}}_{mu}$  (dotted line) for Eqs. (5.12), with parameter values  $\lambda = -0.1833$ ,  $\mu = 0.75$ ,  $\nu = 0$  and initial conditions  $\boldsymbol{\xi} = (0.01, 0.015, -0.018)$ . For comparison, the dashed line decreases as  $\exp(-2(\lambda_u - \lambda_m)t) \simeq \exp(-2(0.698 - 0.271)t) = \exp(-0.854t)$ .

FIG. 6.  $\tilde{\mathcal{H}}_{um}$  and  $\tilde{\mathcal{H}}_{mu}$  (respectively the solid and dotted lines, which lie on top of each other) for Eqs. (5.12), with parameter values  $\lambda = 0.1833$ ,  $\mu = 0.75$ ,  $\nu = -2.6667$  and initial conditions  $\boldsymbol{\xi} = (0.01, 0.015, -0.018)$ . For comparison, the dashed line decreases as  $\exp(-2(\lambda_u - \lambda_m)t) \simeq \exp(-2(0.396 + 0.159)t) = \exp(-1.11t)$ . The noisiness after  $t \simeq 22$  is due to roundoff error.

FIG. 7.  $\tilde{\mathcal{H}}_{uu}$  (solid line) for Eqs. (5.12), with the same parameter values and initial conditions as in Fig. 5. The dashed line has the same slope as in Fig. 5.

FIG. 8.  $\tilde{\mathcal{H}}_{uu}$  (solid line) for Eqs. (5.12), with the same parameter values and initial conditions as in Fig. 6. The dashed line has the same slope as in Fig. 6.

FIG. 9. Top: Plot of  $\hat{\mathbf{u}} \cdot \nabla \times \hat{\mathbf{m}}$  (solid line) and  $\hat{\mathbf{s}} \cdot \nabla \lambda_m t$  (dotted line) versus time for  $A = 5$ ,  $B = C = 2$  flow [Eqs. (5.13)], with initial conditions  $\boldsymbol{\xi} = (0.5, 0.3, 0.3232)$ . The convergence of the two lines verifies the constraint (5.3). Bottom: Plot of  $\hat{\mathbf{m}} \cdot \nabla \times \hat{\mathbf{u}}$  (solid line) and  $-\hat{\mathbf{s}} \cdot \nabla \lambda_u t$  (dotted line) versus time for the same flow. The convergence of the two lines verifies the constraint (5.4).

FIG. 10. Log-linear (base 10) plot of  $\tilde{\mathcal{H}}_{um}$  (solid line) and  $\tilde{\mathcal{H}}_{mu}$  (dotted line) versus time for  $A = 5$ ,  $B = C = 2$  flow [Eqs. (5.13)], with initial conditions as in Fig. 9. There are large fluctuations, but the trend is for both terms to go to zero; they have reached values of  $10^{-7}$  at  $t = 12$ . Note that, from Fig. 9, the terms that cancel to give exponential convergence to zero are roughly of order one, so they agree to about seven digits. For comparison, the dashed line decreases like  $\exp(-2(\lambda_u - \lambda_m)t) \simeq \exp(-2t)$ .

FIG. 11. Top: Plot of  $\tilde{\mathcal{H}}_{uu}$  (solid line),  $\tilde{\mathcal{H}}_{mm}$  (dashed line),  $\tilde{\mathcal{H}}_{ss}$  (dotted line, lying on top of  $\tilde{\mathcal{H}}_{mm}$ ) versus time for  $A = 5$ ,  $B = C = 2$  flow [Eqs. (5.13)], with initial conditions as in Fig. 9. For this particular system, with these parameters, we have  $\tilde{\mathcal{H}}_{mm} = \tilde{\mathcal{H}}_{ss}$ , though this does not appear to be generic. Bottom: Log-linear (base 10) plot of  $\tilde{\mathcal{H}}_{uu} = \hat{\mathbf{u}} \cdot \nabla \times \hat{\mathbf{u}}$ , showing its exponential convergence to zero—as predicted by the constraint (5.5). For comparison, the dashed line decreases like  $\exp(-2(\lambda_u - \lambda_m)t) \simeq \exp(-2t)$ .

FIG. 12. Top: Plot of  $\hat{\mathbf{u}} \cdot \nabla \times \hat{\mathbf{m}}$  (solid line) and  $\hat{\mathbf{s}} \cdot \nabla \lambda_m t$  (dotted line) versus time for the Lorenz model [Eqs. (5.14)], with parameter values  $\sigma = 10$ ,  $b = 8/3$ ,  $r = 28$ , and initial conditions  $\boldsymbol{\xi} = (0, 1, 0)$ . Bottom: Plot of  $\hat{\mathbf{m}} \cdot \nabla \times \hat{\mathbf{u}}$  (solid line) and  $-\hat{\mathbf{s}} \cdot \nabla \lambda_u t$  (dotted line) versus time for the same flow. In both plots the two lines initially seem to converge but then diverge abruptly before converging again at  $t \simeq 21$ . This is due to the trajectory approaching an unstable fixed point of the model and undergoing nearly-periodic motion. During that time the trajectory does not “feel” the chaos, and only after it leaves the vicinity of the fixed point does convergence of  $\tilde{\mathcal{H}}_{um}$  and  $\tilde{\mathcal{H}}_{mu}$  resume. (see Fig. 13.)

FIG. 13. Log-linear (base 10) plot of  $\tilde{\mathcal{H}}_{um}$  (solid line) and  $\tilde{\mathcal{H}}_{mu}$  (dotted line) versus time for the Lorenz model with the same parameter values as in Fig. 12. As mentioned in Fig. 12, the trajectory is initially nearly-periodic. It has to first get away from the unstable fixed point and explore the attractor before the convergence really sets in, at  $t \simeq 20$ .

FIG. 14. Top: Plot of  $\tilde{\mathcal{H}}_{uu}$  (solid line) and  $\tilde{\mathcal{H}}_{mm}$  (dashed line) versus time for the Lorenz model with the same parameter values as in Fig. 12. For this particular system, with these parameters, we have  $\tilde{\mathcal{H}}_{mm} = \tilde{\mathcal{H}}_{ss}$ , though this does not appear to be generic. Bottom: Log-linear (base 10) plot of  $\tilde{\mathcal{H}}_{uu} = \hat{\mathbf{u}} \cdot \nabla \times \hat{\mathbf{u}}$ , showing its exponential convergence to zero—as predicted by the constraint (5.5). See the caption to Figs. 12 and 13 and the text for a discussion on the transient oscillations before convergence sets in.

FIG. 15. Top: For the system of oscillating convection rolls, a plot of the magnitude of the curvature of the  $\hat{\mathbf{s}}$  line,  $\boldsymbol{\kappa} = (\hat{\mathbf{s}} \cdot \nabla)\hat{\mathbf{s}}$ , as a function of the distance  $\tau$  along the  $\hat{\mathbf{s}}$  line labeled  $A$  to  $B$  in Fig. 1 (with the same parameter values). Bottom: Plot of the finite-time Lyapunov exponent  $\lambda$  at  $t = 7$  for the same system, as a function of  $\tau$ . Note the correlation between the locally small values of  $\lambda$  and the magnitude of the curvature  $\boldsymbol{\kappa}$ .

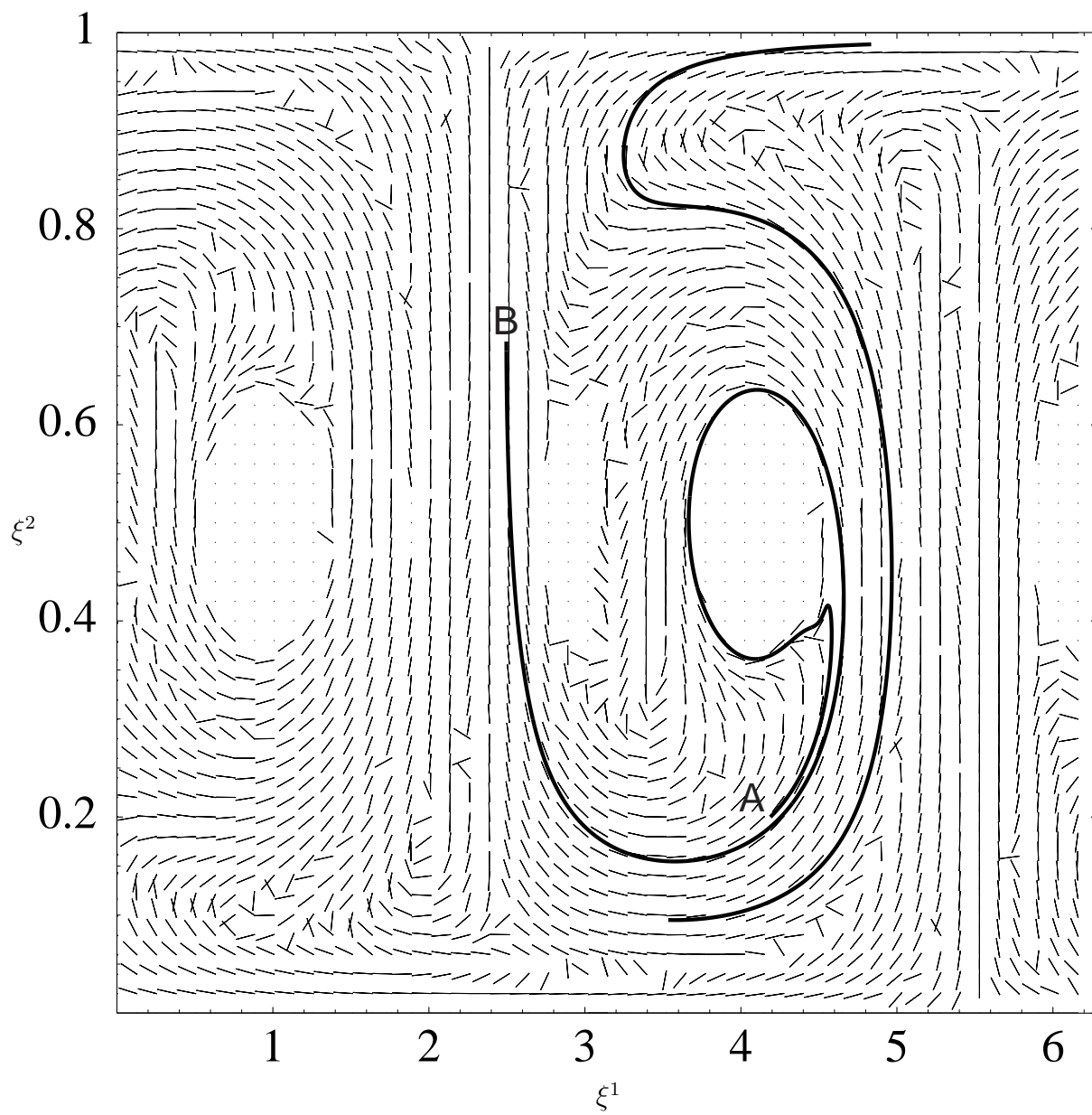


Fig. 1

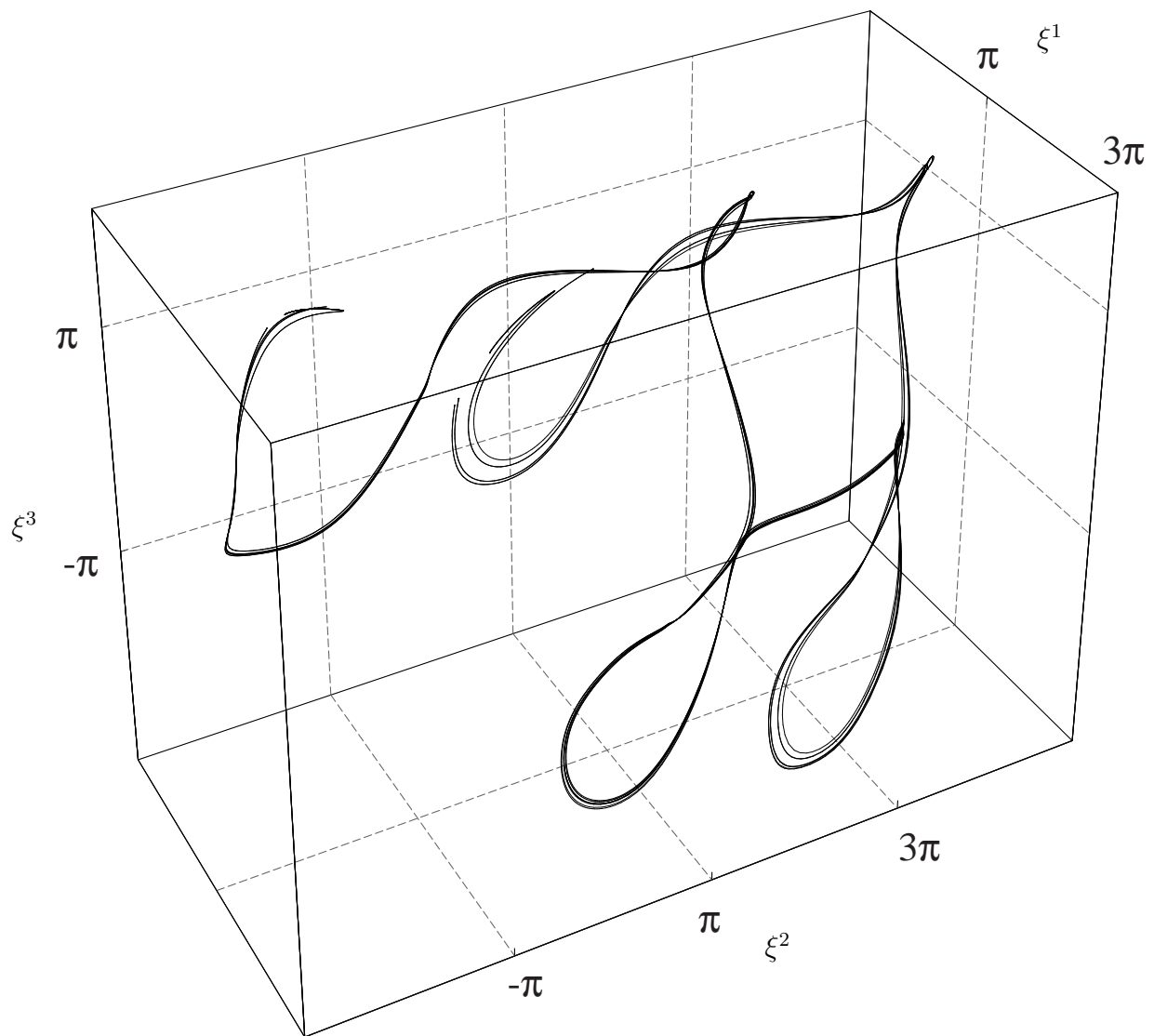


Fig. 2

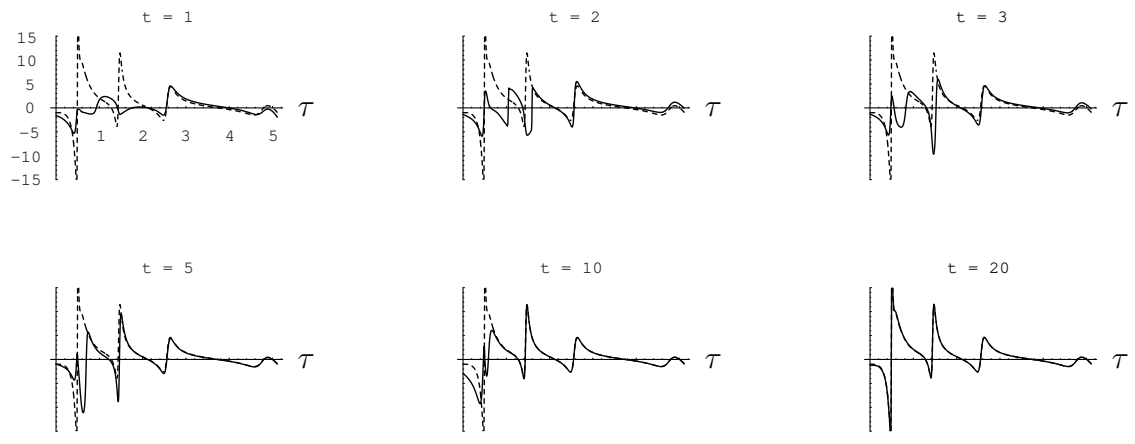


Fig. 3



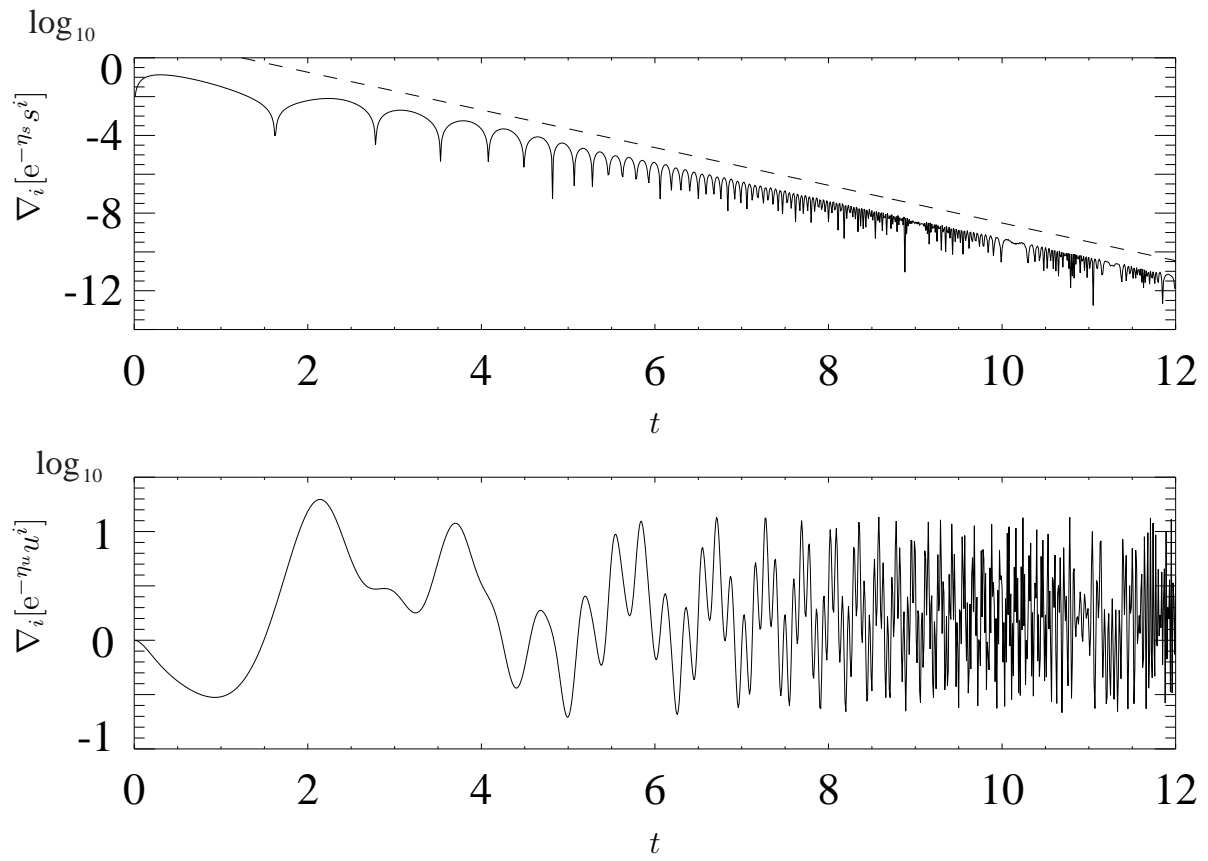


Fig. 4

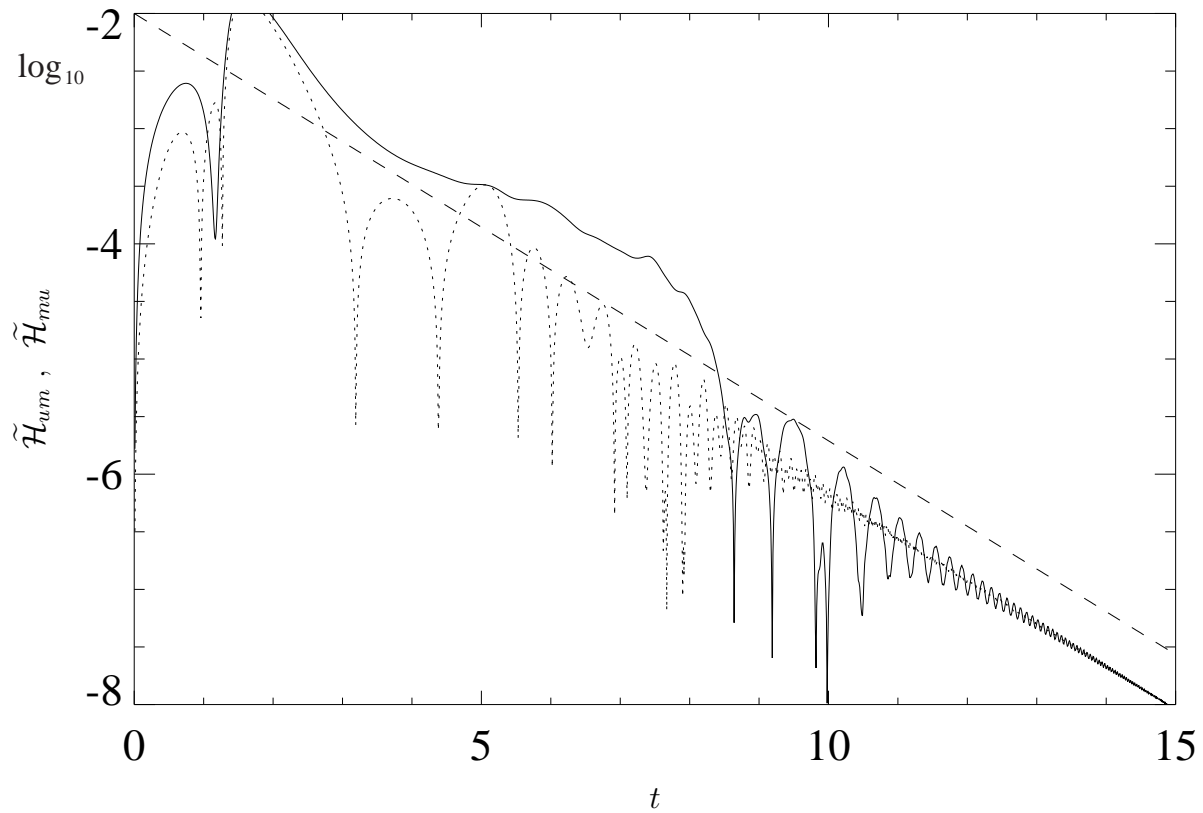


Fig. 5

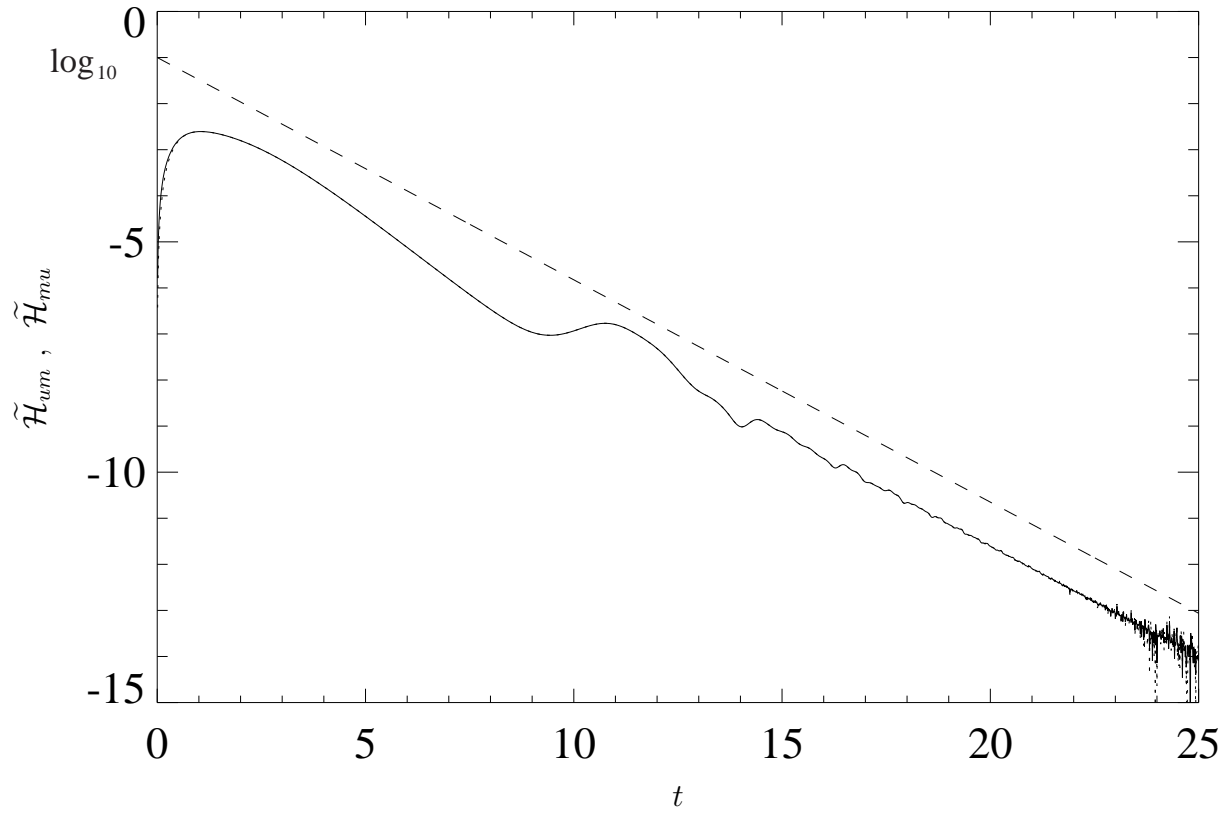


Fig. 6

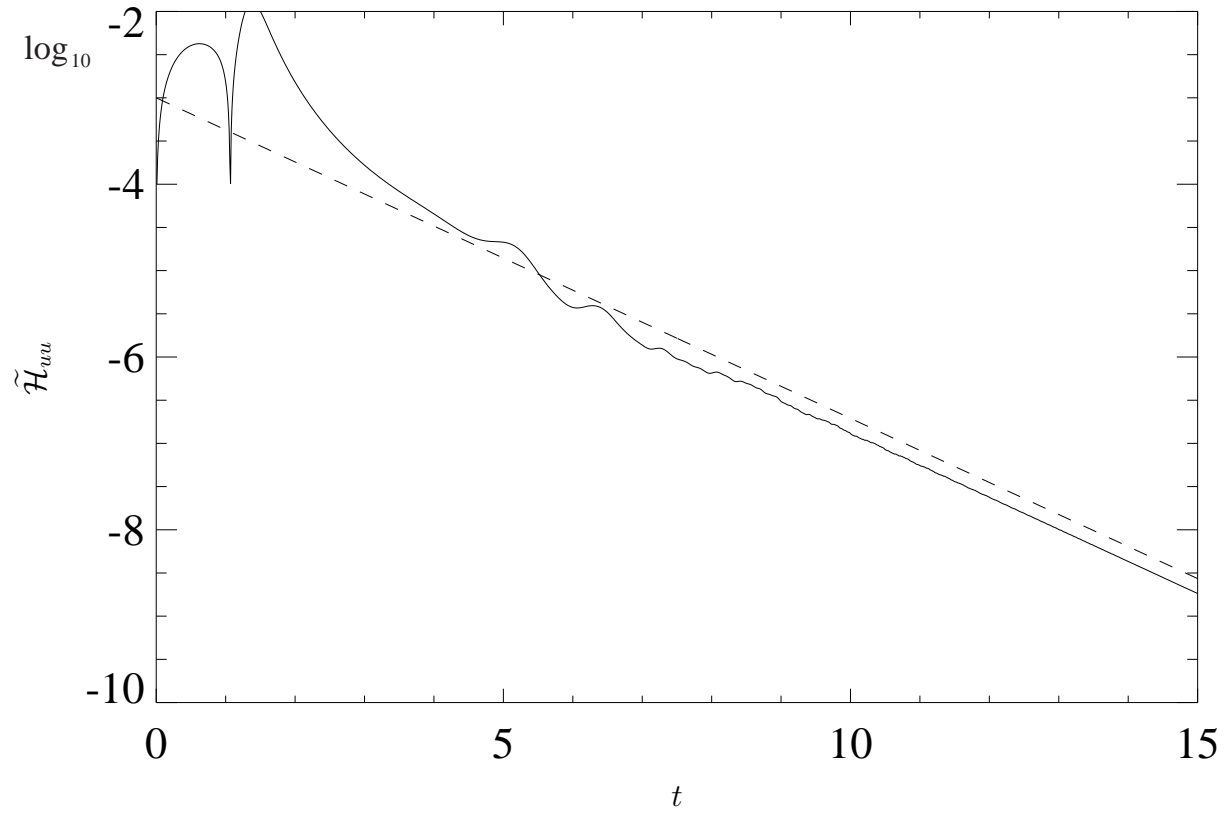


Fig. 7

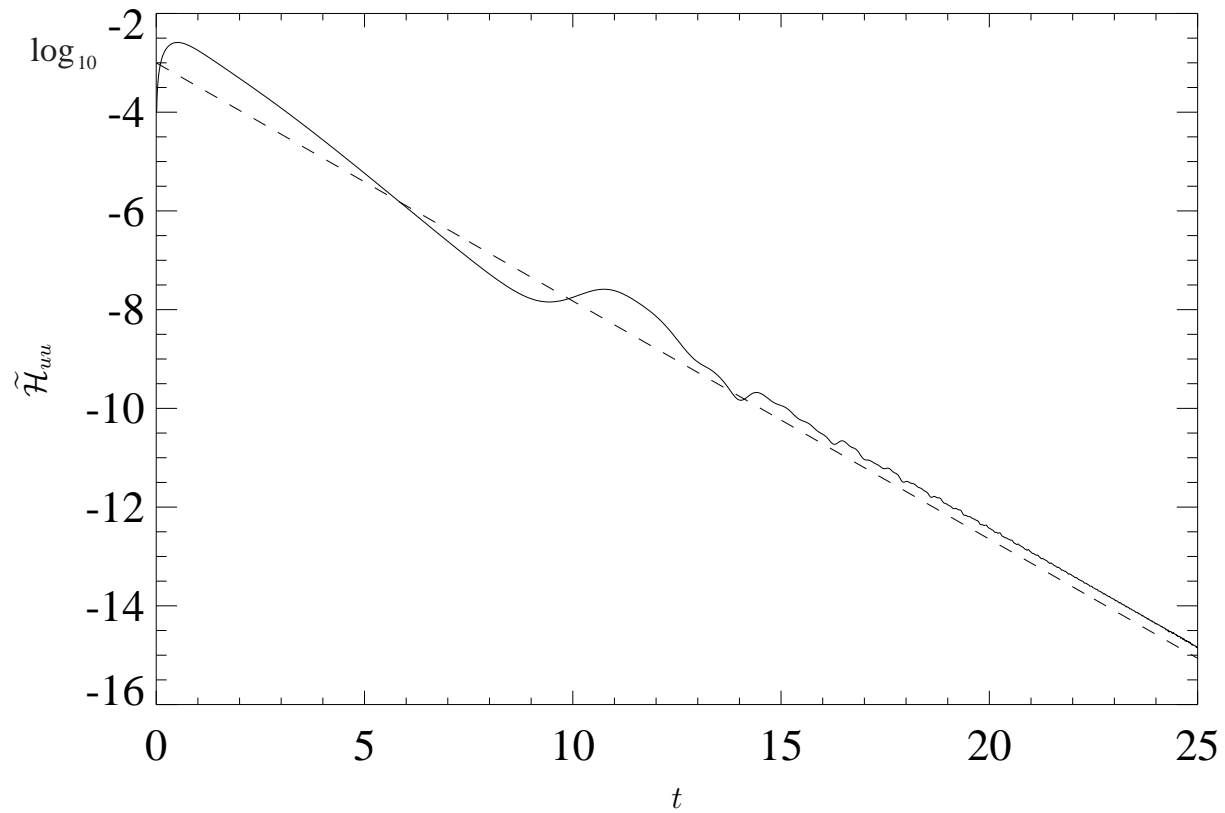


Fig. 8

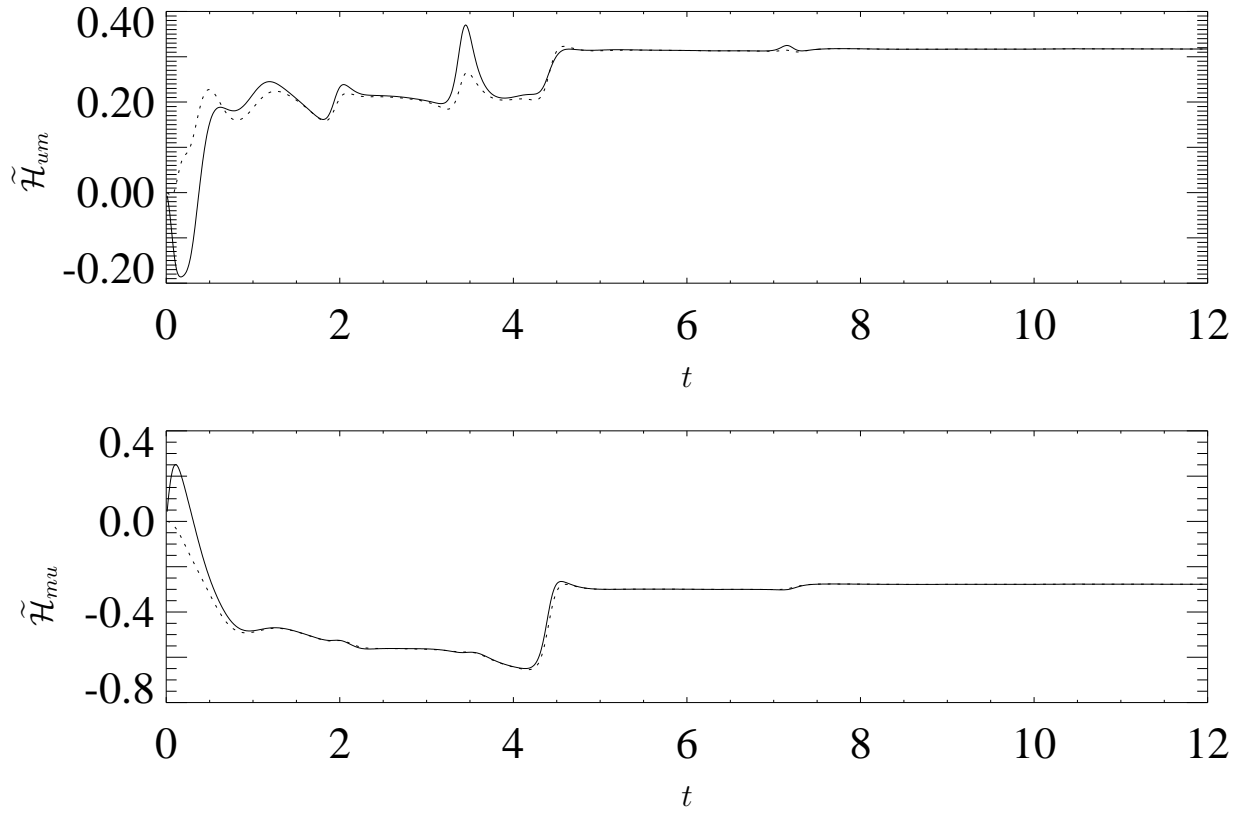


Fig. 9

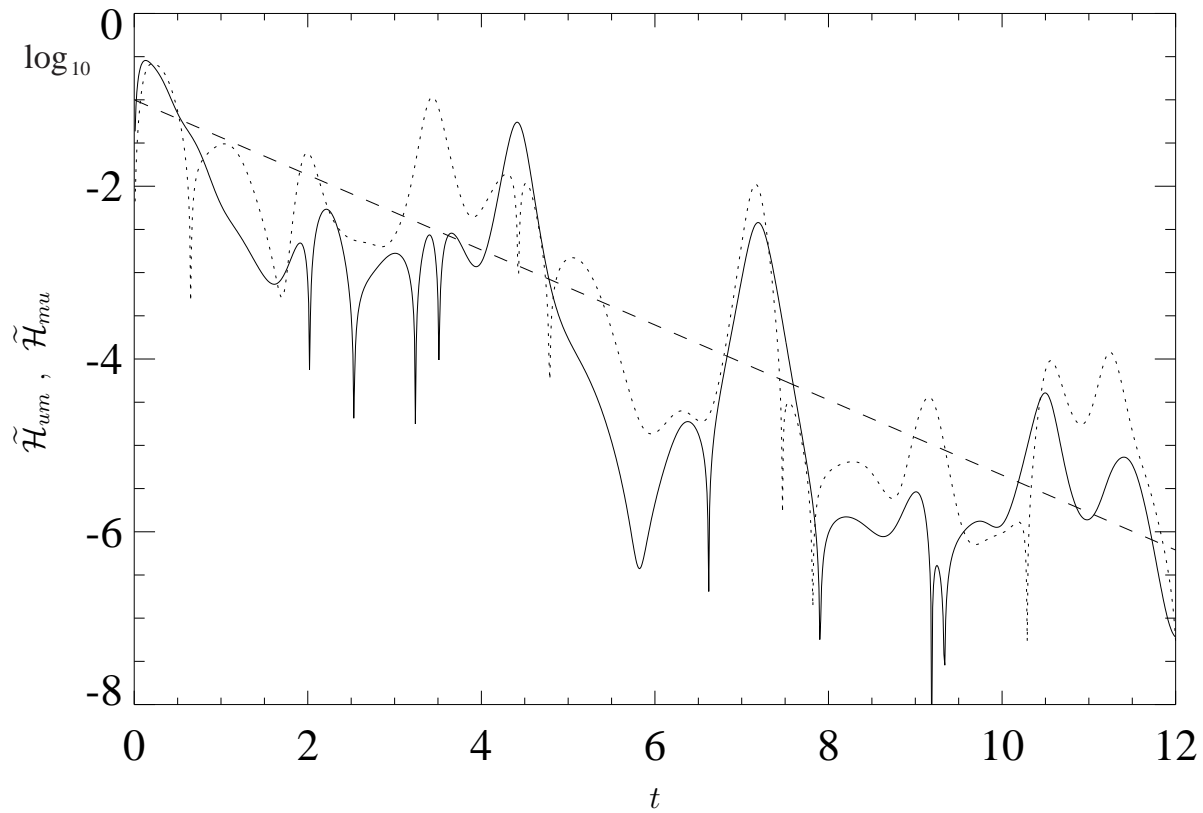


Fig. 10

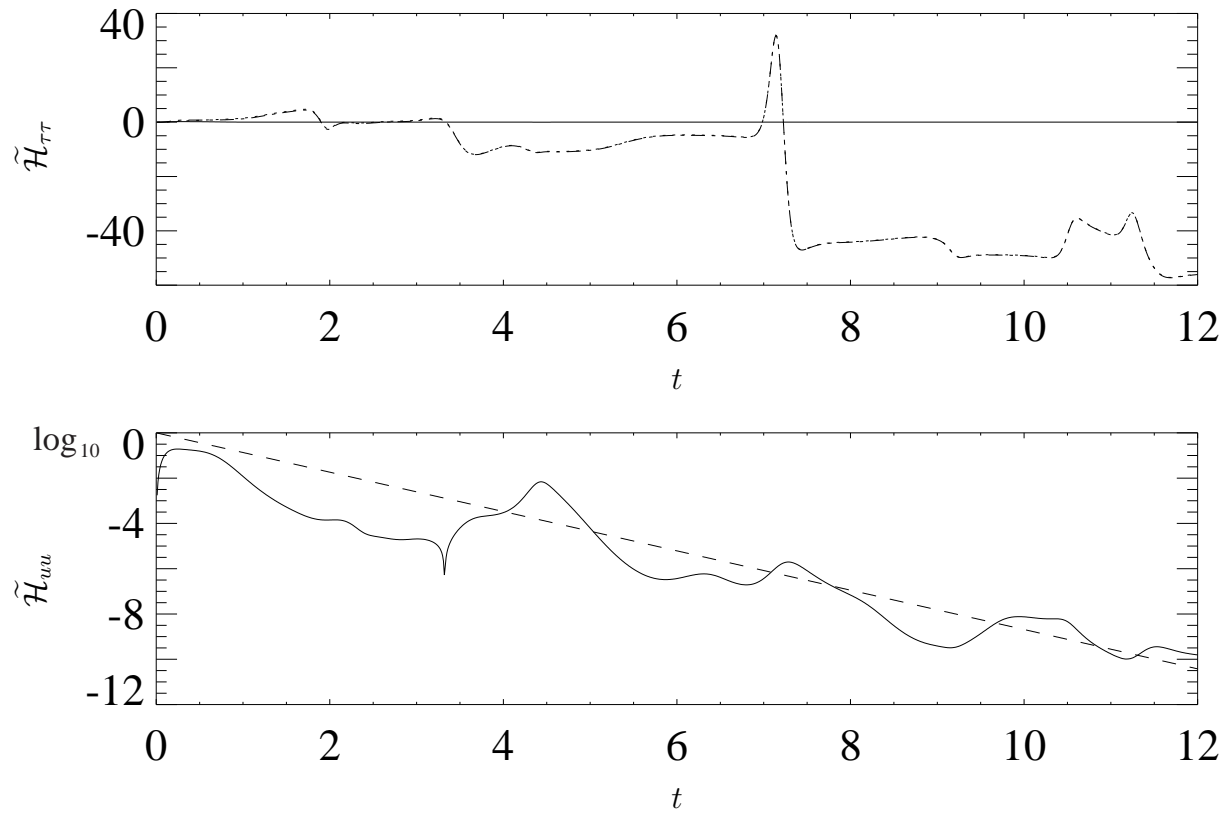


Fig. 11



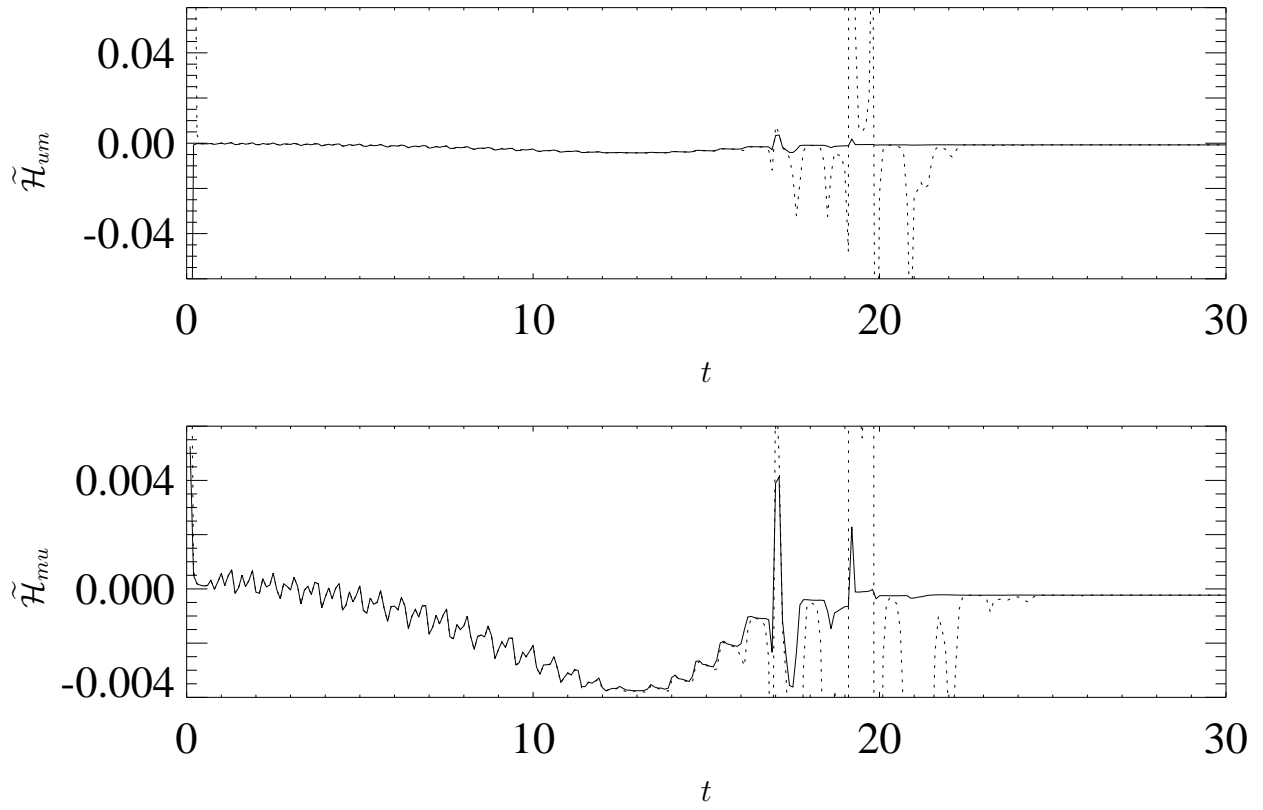


Fig. 12

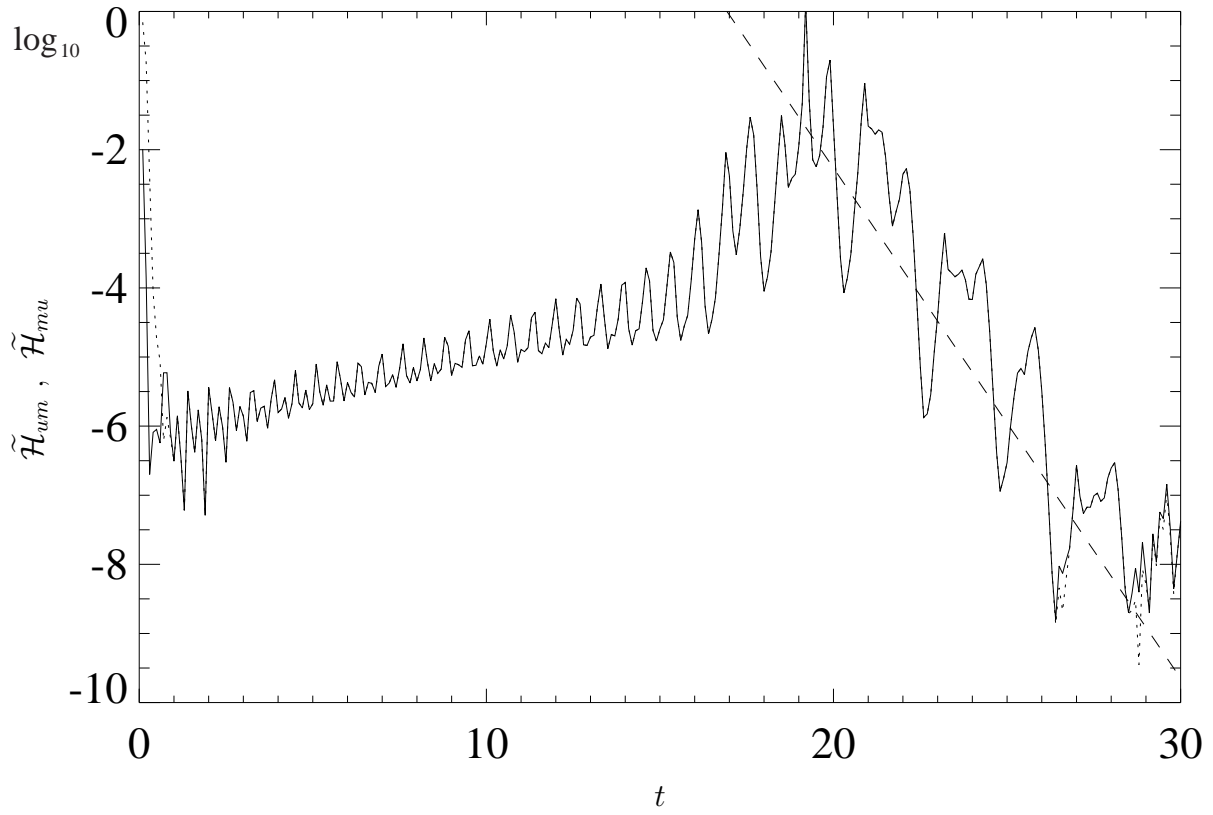


Fig. 13

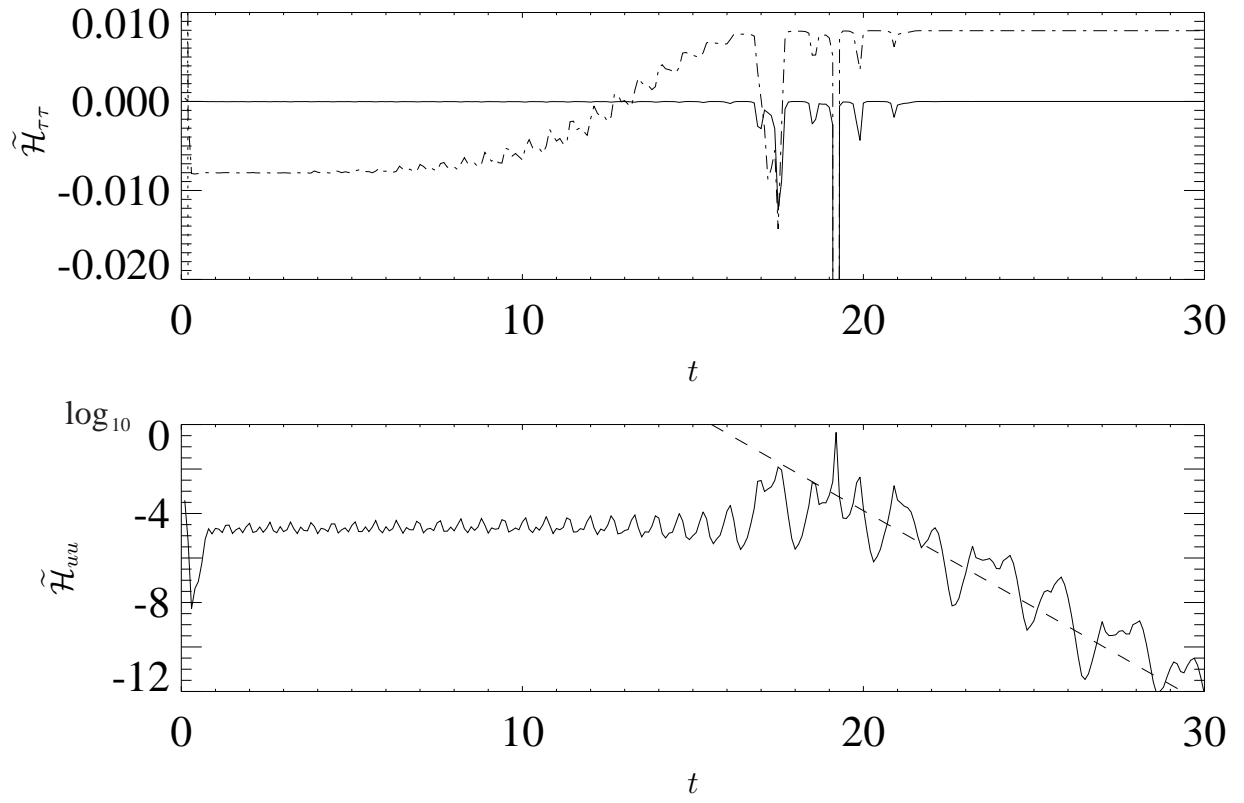


Fig. 14

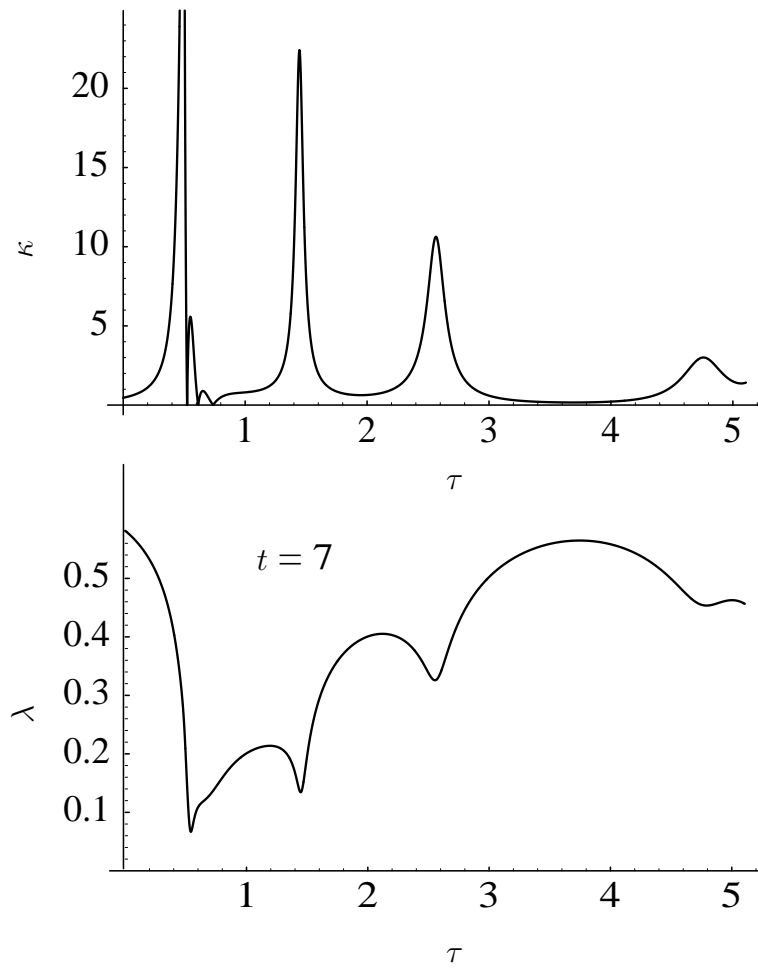


Fig. 15